



## Geomorphic signatures of the transient fluvial response to tilting

Helen W. Beeson<sup>1</sup> and Scott W. McCoy<sup>1</sup>

<sup>1</sup>Department of Geological Sciences and Engineering, University of Nevada, Reno, NV, 89557 USA

**Correspondence:** Helen W. Beeson (hbeeson@nevada.unr.edu)

**Abstract.** Nonuniform rock uplift in the form of tilting has been documented in convergent margins, postorogenic landscapes, and extensional provinces. Despite the prevalence of tilting, the transient fluvial response to tilting has not been quantified such that tectonic histories involving tilt can be extracted from river network forms. We used numerical landscape evolution models to characterize the transient erosional response of a river network initially at equilibrium to a punctuated rigid-block tilting event. Using a model river network composed of linked 1-D river longitudinal profile evolution models, we show that the transient response to punctuated tilting creates characteristic forms or geomorphic signatures in mainstem and tributary profiles that are distinct from those generated by other perturbations such as a step change in uniform rock uplift rate or major truncation of headwater drainage area that push a river network away from equilibrium. These signatures include 1) a knickpoint in the mainstem that separates a downstream profile with uniform steepness (i.e., channel gradient normalized for drainage area) from an upstream profile with nonuniform steepness, with the mainstem above the knickpoint more out of equilibrium than the tributaries following forward tilting towards the outlet, versus the mainstem less out of equilibrium than the tributaries following back tilting towards the headwaters; 2) a pattern of mainstem incision below paleotopography markers that increases linearly up to the mainstem knickpoint, or vice-versa following back tilting; and 3) tributary knickzones with nonuniform steepness that mirrors that of the mainstem upstream of the slope-break knickpoint.

Immediately after tilting, knickpoints form at the mainstem outlet and each mainstem-tributary junction. Time since tilting onset is recorded by mainstem knickpoint location relative to base level and by the upstream end of tributary knickzones relative to tributary-mainstem junctions. Tilt magnitude is recorded in the spatial gradient of mainstem incision depth and, in the forward tilting case, by tributary knickzone drop height. Heterogeneous lithology can modulate the transient response to tilting and, post-tilt, knickpoints can form anywhere in a stream network where more erodible rock occurs upstream of less erodible rock. With a full 2-D model, we show that stream segments flowing in the tilt direction have elevated channel gradient during the transient and that the magnitude of tilt can be recovered from the relationship between channel gradient and azimuth, but only shortly after tilting. Tilting is also reflected in network topologic changes via stream capture oriented in the direction of tilt. As an example of how these geomorphic signatures can be used in concert to estimate timing and magnitude of a tilting event, we show a sample of rivers draining the west slope of the Sierra Nevada, California, USA, a range long thought to have been tilted westward towards river outlets in the late Cenozoic.



## 1 Introduction

In unglaciated mountainous terrain, bedrock rivers are the primary drivers of landscape evolution (Howard, 1994). Bedrock rivers evolve in response to external forcing, including rock uplift rate and climate, set base level for bounding hillslopes and the steep headwater valley network where debris flows can dominate, define the relief structure of the landscape as it is carved into valleys and ridges, and can transmit changes in external forcing through the river network (Burbank et al., 1996; Howard, 1994; Howard and Kerby, 1983; Ouimet et al., 2009; Snyder et al., 2000; Stock and Dietrich, 2003; Whipple, 2004; Whipple and Tucker, 1999). The channel steepness index, or the rate at which channel slope changes with drainage area (Hack, 1957; Flint, 1974), of rivers that have reached an equilibrium grade (Mackin, 1948) has been shown to reflect spatial patterns in uplift rate, millennial-scale erosion rates, rock erodibility, and climate (e.g., Bonnett and Crave, 2003; DiBiase et al., 2010; Duvall et al., 2004; Ouimet et al., 2009; Snyder et al., 2000; Wobus et al., 2006). Transient river profiles can record discrete, persistent, or cyclic changes in climate, lithology, relative base level, or drainage area as the river profile adjusts to the changes and evolves towards an equilibrium state that reflects modern boundary conditions (Whipple, 2013). Knowledge of the transient response of bedrock rivers to different perturbations thus comprises an important geomorphic tool to characterize the history of rock uplift rates, climate, or changes in river network topology from disequilibrium landscape form (e.g., Beeson et al., 2017; Ferrier et al., 2013; Kirby and Whipple, 2012; Lease and Ehlers, 2013; Tucker and Whipple, 2002; Whittaker et al., 2008; Willett et al., 2014; Wobus et al., 2006). Such histories are critical for testing geodynamic models of orogenesis and quantifying the relative importance of external forcing, such as climate and tectonics, versus internal complex system response, on the evolution of mountainous landscapes (e.g., Beeson et al., 2017; Clark et al., 2005; Gallen, 2018; Kirby and Whipple, 2012; Whipple et al., 2017; Willett et al., 2018; Yang et al., 2015).

Previous studies have illustrated the expected transient response in bedrock rivers to step changes in uniform rock erodibility or uplift rate (Baldwin et al., 2003; Bonnet and Crave, 2003; Howard, 1994; Royden and Perron, 2013; Tucker and Whipple, 2002; Whipple and Tucker, 1999), sudden base-level fall or uniform pulses of rock uplift (Grimaud et al., 2016; Rosenbloom and Anderson, 1994; Whipple and Tucker, 1999), erosion through layered stratigraphy (Forte et al., 2016), and cyclic fluctuations in rock erodibility, base level, or uplift rate (Goren et al., 2016; Snyder et al., 2002). Kirby and Whipple (2001) predict that steady-state bedrock rivers adjusted to uplift gradients with maximum uplift either at the channel head or the channel outlet will have increased and decreased concavities, or the rate of change of river slope with distance downstream, respectively. Whittaker et al. (2008) and Attal et al. (2011) explore the transient response to a step increase in nonuniform uplift rate on fault-bounded tilted blocks, but with a primary focus on how different erosion formulations modulate the mainstem response. Despite this progress, well-defined characteristics of the transient response across an entire bedrock river network to nonuniform uplift owing to a punctuated tilting event is still lacking.

Nonuniform rock uplift in the form of tilting has been documented across tectonic settings. Convergent boundaries where tilting has been documented include the western flank of the central Andes (Farías et al., 2005; Jordan et al., 2010; Lamb and Hoke, 1997; Saylor and Horton, 2014; Wörner et al., 2002), the Siwalik Hills in the foothills of the Himalaya (Delcaillau et al., 2007; Kirby and Whipple, 2001; Lavé and Avouac, 2000; Singh and Tandon, 2007), and the Manawatu region of northern New



Zealand (Jackson et al., 1998). In the postorogenic North American Cordillera, regional tilting has been documented in the Sierra Nevada (Huber 1981; Jones, 2004; Lindgren, 1911; Unruh, 1991; Wakabayashi, 2013; Wakabayashi and Sawyer, 2001), the Rocky Mountains (McMillan et al., 2002; Riihimaki et al., 2007), the Salmon River basin (Mitchell and Yanites, 2019), and the Colorado Plateau (Liu and Gurnis, 2010; Moucha et al., 2009, Moucha et al., 2008; Sahagian et al., 2002). Tilting on a smaller scale has been documented on fault-bounded blocks in extensional terrain in the Appenines (Whittaker et al., 2008 and references therein) and throughout the Basin and Range (Stewart, 1980), including the Teton Range (Byrd et al., 1994), the Wassuk Range (Gorynski et al., 2013), the White Mountains (Stockli et al., 2003), and the Wasatch Range (Armstrong et al., 2003). Although tilting is widely documented, characteristic forms of bedrock rivers during the transient response to tilting have yet to be quantified.

Here, we seek to answer the question: *What are the geomorphic signatures of the transient fluvial response to tilting and can these signatures be used to quantify uplift histories in terms of timing and magnitude?* We focus on tilting towards the river outlet in which the mainstem river network is everywhere steepened by tilting about a horizontal axis located at the river outlet and oriented perpendicular to the mainstem (referred to throughout as forward tilting), though we simulate the transient response to other tilt directions relative to the mainstem flow direction to highlight general patterns. Specifically, we simulated forward, back (i.e., tilting about a horizontal axis located at the channel head and oriented perpendicular to the mainstem) and side tilting (i.e., tilting about a horizontal axis located along the mainstem and oriented parallel to the mainstem) in homogeneous lithology and forward tilting with the simplest case of vertically-bedded heterogeneous lithology. Additionally, we explore perturbations that generate river profiles with similar characteristics to those produced by tilting. Many of these perturbations likely generate depositional signatures as well, but in this paper we focus exclusively on the erosional response in bedrock rivers. Although uplift histories in nature are diverse and might involve various permutations of uniform and nonuniform uplift fields, we focus on the simple case of a single short-duration rigid-block tilting event that increases rock and surface uplift rates well above background rates. Lastly, we document the expression of geomorphic signatures of a punctuated rigid-block tilting event proposed to have occurred in the Sierra Nevada of California, USA (Huber 1981; Jones, 2004; Lindgren, 1911; Unruh, 1991; Wakabayashi, 2013) and demonstrate how these signatures can be applied to estimate the timing and magnitude of tilt.

## 2 Methods

We used 1- and 2-dimensional (1- and 2-D) numerical landscape evolution modeling to explore the transient response of river longitudinal profiles and river networks to various perturbations that move a river away from equilibrium, with particular emphasis on punctuated rigid-block forward tilting, and then compared these results with topographic analysis of river geomorphology on the western slope of the Sierra Nevada, a range proposed to have been tilted westward in the late Cenozoic. For the topographic analysis of the Sierra Nevada, we used 3 arc-second (~90 m) digital elevation models (DEMs) derived from the Shuttle Radar Topography Mission and downloaded from Open Topography (<http://opentopography.org>). We clipped the DEM of the Sierra by the crest on the eastern side and by the mountain front on the western side. We identified the mountain



front using a threshold slope of 0.01 on a DEM that was smoothed with a 20 km moving window. To map the river network in the DEM of the Sierra as well as in simulated DEMs, we calculated flow direction and accumulation using a steepest descent flow algorithm. All topographic analysis on real and simulated DEMs was completed using the Matlab-based software package TopoToolbox (Schwanghart and Scherler, 2014).

## 5 2.1 Numerical landscape evolution modeling

For all numerical models, we used the stream power model of bedrock incision, which assumes the rate of bedrock incision is proportional to the stream power per unit channel width and that incision is limited by the rate at which the river can detach bedrock particles, as opposed to the rate at which detached particles can be transported (Howard, 1994; Perron et al., 2008; Siedl and Dietrich, 1992; Whipple, 2004; Whipple and Tucker, 1999). To simulate the evolution of the land surface we numerically solved the following governing equation using a forward-time finite-difference solver:

$$\begin{aligned} \frac{\delta z}{\delta t} &= U - KA^m |\nabla z|^n & |\nabla z| \leq S_c \\ \frac{\delta z}{\delta t} &= U - \xi_l & |\nabla z| > S_c \end{aligned} \quad (1)$$

where  $z$  is land surface elevation,  $t$  is time,  $U$  is rock uplift rate relative to base level,  $K$  is an erodibility coefficient,  $A$  is drainage area,  $m$  and  $n$  are empirical constants,  $S_c$  is a critical gradient above which landsliding is initiated, and  $\xi_l$  is the erosion rate required to reduce slopes to  $S_c$  across the domain in a single time step. The equation in the bottom row imposes a maximum hillslope gradient and is a simple representation of threshold-controlled landsliding in which rock required to decrease gradient down to  $S_c$  is removed from each over-steepened cell through an iterative process during each time step until the gradient of all grid cells in the domain is less than or equal to  $S_c$ .

To simulate just the evolution of a river longitudinal profile, the problem is one-dimensional, and equation 1 can be simplified to

$$20 \quad \frac{\delta z(x,t)}{\delta t} = U(x,t) - K(x,t)A(x,t)^m \left| \frac{dz(x,t)}{dx} \right|^n \quad (2)$$

where  $x$  is distance along the river. Equation 2 is only valid some distance down slope,  $x_c$ , of the drainage divide where fluvial processes are active. In these 1-D river profile models we assumed drainage area along the channel can be described using Hack's law,  $A = k_a x^h$ , where  $k_a$  and  $h$  are empirical constants (Hack, 1957). Equations 1 and 2 take the form of a nonlinear wave equation with a source term  $U$  and thus perturbations to river profile slope move up through a river network in a wave-like manner with celerity,  $C$ , dependent on erodibility,  $K$ , and drainage area,  $A$ , as well as river slope,  $S = dz/dx$  in 1-D, if  $n$  is not unity such that  $C = KA^m S^{n-1}$  (Tucker and Whipple, 2002). We use the terminology presented by Haviv et al. (2010) and Whipple et al. (2013) to call a point that separates portions of a river profile with dissimilar channel steepness a 'slope-break knickpoint' and a point at which offset of similar steepness channel profiles occurs a 'vertical-step knickpoint'. We use 'knickzone' to denote a portion of the river profile that has locally high channel steepness.



## 2.2 $\chi$ and $\chi$ plots for identifying equilibrium and transients in river profiles

For rivers in simulated topography and in the Sierra Nevada, we calculated the channel length-drainage area scaling relationship,  $\chi$ , that can be derived by solving equation 2 for steady-state or equilibrium conditions with uniform rock uplift rate,  $U$ , and rock erodibility,  $K$ .

$$z(x) = z_b + \left( \frac{U}{KA_0^n} \right)^{\frac{1}{n}} \chi \quad (3)$$

where

$$\chi = \int_{x_b}^x \left( \frac{A_0}{A(x')} \right)^{\frac{n}{n-1}} dx' \quad (4)$$

We define steady-state or equilibrium for a bedrock river as the state in which the time rate of change of river profile elevation is equal to zero, which occurs once river network area and slope adjust such that there is a perfect balance between input of rock by rock uplift relative to base level and removal of rock by erosion. For these conditions, equation 3 shows that river elevation scales linearly with  $\chi$ . An equilibrium river profile with uniform rock uplift rate and erodibility will be linear on a  $\chi$  plot (i.e., a plot of river elevation as a function of  $\chi$ ) rather than curved, as it would be in an untransformed longitudinal profile (Perron and Royden, 2013). Thus  $\chi$  can be used as a proxy for the steady-state elevation of the river network, as well as a convenient transformation variable that removes the effect of basin geometry and the downstream increase in drainage area on river longitudinal profile shape (Perron and Royden, 2013; Willett et al., 2014). Tributaries in equilibrium with the same uplift rate and with the same erodibility as the mainstem will be co-linear with each other as well as with the mainstem such that all portions of an equilibrium river network collapse towards a single straight line on a  $\chi$  plot.

Deviations from a linear  $\chi$  plot can be used to identify river profiles in a state of transient adjustment in response to changes in rock uplift rate, rock erodibility, or basin geometry that move a river away from equilibrium or deviations from assumed uniformity in uplift and rock erodibility (Perron and Royden, 2013; Willett et al., 2014).  $\chi$  plots are particularly useful for identifying transient knickpoints propagating through a river network that share a common origin because these knickpoints will collapse to the same  $\chi$  value. In the same manner that transformed profiles remove the effect of downstream increases in drainage area on river longitudinal profile shape, transformed profiles remove drainage area effects on the perturbation travel distances. We exploit these properties of transformed river profiles to identify portions of the river network that are near equilibrium (i.e., linear  $\chi$  plots), versus out of equilibrium (i.e., nonlinear  $\chi$  plots), as well as to test whether transient signals have a common origin (transient signals located at the same point in  $\chi$  space).

With  $A_0 = 1$ , the coefficient in front of the integral quantity  $\chi$  in equation 3 is the channel steepness,  $k_s$  (Perron and Royden, 2013):

$$k_s = \left( \frac{U}{K} \right)^{\frac{1}{n}} \quad (5)$$

and thus  $k_s$  is the slope of a  $\chi$  plot. Throughout the paper we use channel steepness or profile steepness to refer to  $k_s$ . We never use steepness as a synonym of channel gradient.



### 2.3 Estimating time since perturbation

The fluvial response time,  $\tau$ , defined as the time for a perturbation originating at base level to travel to any point on the river network, is given by the upstream integral of the inverse wave speed:

$$\tau = \int_{x_b}^x \frac{1}{KA^m S^{n-1}} dx \quad (6)$$

- 5 When  $K^n A_0^m$  is included in the integral in equation 4,  $\chi$  has units of time and the integral yields the fluvial response time (Whipple and Tucker, 1999; Willett et al., 2014). Thus, if  $n = 1$  and  $K$  is uniform,  $\tau$  is simply  $\frac{\chi}{K}$ . For other cases of  $n$ ,  $\tau$  can be estimated analytically for quasi-equilibrium river profiles by solving for slope under steady-state conditions in equation 2 (Willett et al., 2018), such that

$$S \approx \left(\frac{U}{K}\right)^{\frac{1}{n}} A^{-\frac{m}{n}} \quad (7)$$

- 10 Substituting equation 7 into equation 6 gives the following expression for  $\tau$

$$\tau \approx k_s \frac{\chi}{U} \quad (8)$$

We used 1-D simulations to explore more quantitatively how deviations away from  $n = 1$  may influence  $\tau$  values estimated for real landscapes if it is assumed in all calculations that  $n = 1$ .

### 2.4 Parameter values

- 15 We selected common values from published studies for all parameters in the stream power model of bedrock incision. The concavity index,  $\theta = m/n$ , has been shown to commonly range between 0.4 – 0.7 for equilibrium channels (Stock and Montgomery, 1999; Tucker and Whipple, 2002; Whipple and Tucker, 1999), with the slope exponent,  $n$ , ranging between 2/3 and 5/3, depending on the erosional mechanism (Whipple et al., 2000). We chose a reference concavity index,  $\theta_{ref}$ , of 0.45 for all simulations and for calculating  $\chi$  and  $k_s$  in the Sierra. Thus  $k_s$  as calculated in equation 5 is equivalent to the normalized  
20 channel steepness index,  $k_{sn}$ , as described by Wobus et al. (2006), and hereafter will be referred to as such. For simplicity we assume  $n = 1$  for all simulations and analyses. However, we also ran 1-D simulations with both  $n = 2/3$  and  $n = 5/3$  and present these results in the supplement. For  $n \neq 1$  simulations we adjusted  $m$  and  $K$  such that both concavity and fluvial relief remained constant between these simulations and those in which  $n = 1$ . We used 6.69 for the reciprocal Hack coefficient,  $k_a$  (Whipple and Tucker, 1999) and 1.8 for the reciprocal Hack exponent,  $h$  (Hack, 1957). We chose a low background rock uplift  
25 rate of 50 mMyr<sup>-1</sup> and a value of  $1 \times 10^{-6}$  m<sup>0.1</sup>yr<sup>-1</sup> for the erodibility coefficient,  $K$ , as this value allows  $\chi$  to be read as response time in millions of years and because it is similar to other published values (e.g., Beeson et al., 2017; Stock and Montgomery, 1999; Willett et al., 2018). To calculate  $\chi$  in the Sierra Nevada, we assumed uniform  $U$  and  $K$ . While we know rock type is nonuniform in the Sierra, we do not know  $K$  for each formation and thus cannot calculate  $\chi$  with local  $K$  values inside the integral (Willett et al., 2014). However, with a 1-D model we demonstrate the signature heterogeneous lithology



would impart on  $\chi$  plots. In the Sierra, we used the mountain front as our base level to limit our analysis to bedrock rivers. We used a scaling area,  $A_0$ , of  $1 \text{ m}^2$  and defined channel heads using a critical drainage area,  $A_c$ , of  $0.5 \text{ km}^2$ .

### 3 Modeling equilibrium fluvial longitudinal profiles

We solved equation 2 analytically to simulate equilibrium fluvial longitudinal profiles for the case where  $U$  is uniformly  $50 \text{ mMyr}^{-1}$  (Fig. 1b) and numerically for the case in which  $U$  is a linear gradient from zero at the channel outlet to a maximum uplift rate of  $50 \text{ mMyr}^{-1}$  at the channel head (Fig. 1c) and for the case with the reverse uplift gradient of maximum uplift rate of  $50 \text{ mMyr}^{-1}$  at the channel outlet to zero at the channel head (Fig. 1d). We used a 200 km long mainstem river with three 40 km long tributaries that entered the mainstem at 20, 80, and 140 km upstream of the outlet (Fig. 1a). The tributaries were made to run perpendicular to the mainstem such that the uplift rate for each tributary was equal to the rate experienced by the mainstem at the tributary confluence.

At steady-state, longitudinal profiles with uniform  $U$  are straight on  $\chi$  plots (Fig. 1b) with the slope equal to the channel steepness, but for the case in which  $U$  is a linear gradient from zero at the channel outlet to a maximum uplift at the channel head, profiles have positive curvature in  $\chi$  plots, particularly near the channel outlet (Fig. 1c). The positive curvature  $\chi$  plot results from channel steepness increasing toward the channel head, which allows erosion rates to increase moving towards the channel head and balance the gradient in rock uplift rate. In contrast, for the case in which  $U$  is a linear gradient decreasing from a maximum at the channel outlet to zero at the channel head (Fig. 1d), longitudinal profiles have negative curvature on a  $\chi$  plot.

### 4 Modeling fluvial longitudinal profile response to perturbations

We solved equation 2 numerically to simulate fluvial longitudinal profile response to various perturbations that move a river away from equilibrium. Specifically, we focus on nonuniform uplift due to forward tilting as well as perturbations that result in disequilibrium profile forms that share characteristics with those generated in response to forward tilting. Starting from initial conditions with equilibrated river profiles, we simulated four main scenarios: 1) an instantaneous uniform pulse of rock uplift that increased the elevation of all points along the river profile 1 km with respect to the outlet; 2) a step decrease in equilibrium profile steepness achieved through either a uniform step increase in bedrock erodibility or a step decrease in uniform rock uplift rate; 3) major truncation or beheading of the mainstem river; and 4) forward tilting owing to an instantaneous rigid-block tilt about a horizontal axis perpendicular to the mainstem river and located at the river outlet that increased the headwater elevation by 1 km with respect to the outlet (tilt of  $\sim 0.3^\circ$ ). For each of these scenarios we conducted analogous simulations but run with  $n = 2/3$  and  $n = 5/3$  and present those results in the supplement.

We simulated four additional tilting scenarios: 1) a forward tilting scenario identical to above but with a vertical bed of more erodible rock mid-profile; 2) a forward tilting scenario identical to above but with a vertical bed of less erodible rock near the outlet; 3) backward tilting owing to an instantaneous rigid-block tilt about a horizontal axis perpendicular to the mainstem river

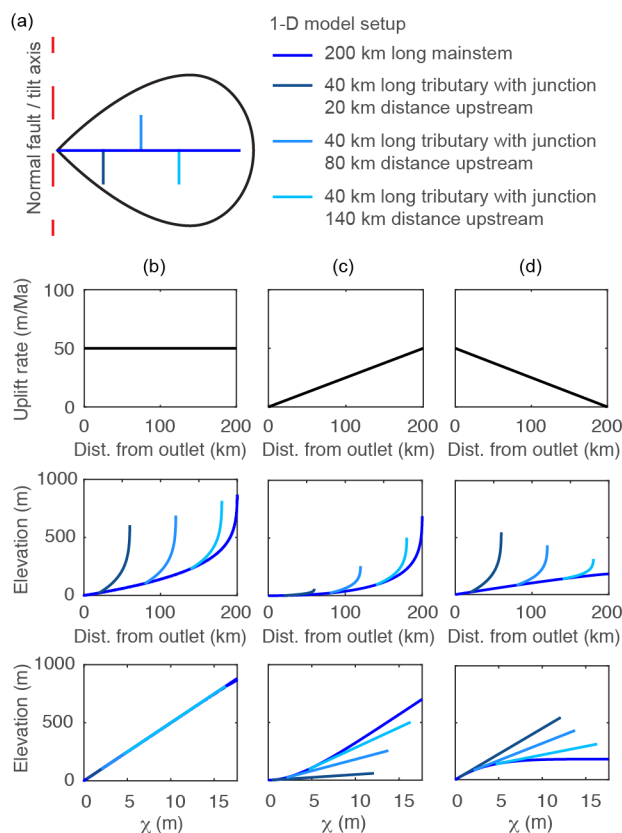


**Figure 1.** Equilibrium river longitudinal profiles. **(a)** Planform schematic of simple river network composed of linked 1-D river-profile models. River profiles equilibrated to **(b)** uniform  $K$  of  $1 \times 10^{-6}$  and uniform  $U$  of  $50 \text{ mMyr}^{-1}$  or **(c)** a linear uplift gradient with maximum  $U$  at the channel head of  $50 \text{ mMyr}^{-1}$ . Upper row shows uplift field, middle row shows longitudinal profiles, and lower row shows  $\chi$  plots.

and located at the channel head that increased channel outlet elevation by 200 m; and 4) an instantaneous rigid-block tilt about a horizontal axis parallel to the mainstem river and located along the mainstem that increased tributary channel heads by 1 km. For all simulations, we imposed a steady, uniform background rock uplift rate of  $50 \text{ mMyr}^{-1}$  and the model setup as described above. For each simulation, we tracked the elevation of the river profile with respect to the river profile immediately after the perturbation to simulate the location of paleoriver deposits as well as incision depth below this paleotopography marker. Animations of all simulations described herein are available as an online resource (see Beeson, 2019).

#### 4.1 Rapid pulse of uniform rock uplift

The transient response to a 1 km instantaneous pulse of uniform rock uplift is illustrated in Figure 2a. The pulse of uniform uplift raises the surface elevation of the equilibrated initial river profile by 1 km and results in a 1 km high vertical-step knickpoint at the outlet. Tributaries and the mainstem are brought above equilibrium (shown as a dashed blue line) by an



equal amount (Fig. 2a middle row). The knickpoint then propagates upstream through the river network in a wave like manner, lowering the fluvial profile by 1 km to return it back to equilibrium. Below the mainstem knickpoint, tributary knickzone height is uniform and equal to the 1 km pulse of rock uplift, which is equal to the surface uplift following the perturbation, whereas incision depth below the uplifted initial river profile is also uniform (Fig. 2a lower row) but equal to the total rock uplift accumulated since the beginning of the simulation (background rate plus 1 km pulse). As highlighted in the  $\chi$  plots (Fig. 2a middle row), at all times during the transient evolution, the knickpoint simply offsets profiles of equal and uniform steepness and each knickpoint within the tributaries and the mainstem collapse to a common  $\chi$  value as expected from their common point of origin. With  $K = 1 \times 10^{-6}$  and uniform,  $\chi$  values of the vertical-step knickpoint can be interpreted as knickpoint travel times,  $\tau$ , in millions of years (Equations 4 and 6) as shown by the knickpoint  $\chi$  value equal to five, which corresponds to  $\tau = 5$  Ma at a time 5 Ma after the uplift perturbation. If  $n = 2/3$  or  $5/3$ , the first-order fluvial response is similar to the case in which  $n = 1$  except that the vertical-step knickpoint broadens with time because of slope-dependent knickpoint celerity (Figs. S1 and S2). The change in celerity with increasing slope also decreases the celerity of the base of the knickpoint in the  $n = 2/3$  case and increases it in the  $n = 5/3$  case as compared to the  $n = 1$  case, increasing and decreasing overall response time, respectively (Figs. S1 and S2).

#### 4.2 Step increase in bedrock erodibility or step decrease in rock uplift rate

The transient response to a step increase in bedrock erodibility,  $K$ , or equivalently a step decrease in uniform rock uplift rate, is illustrated in Figure 2b. To perturb erodibility, the initial condition is a river profile equilibrated to the background uplift rate of  $50 \text{ mMyr}^{-1}$ , but with uniform  $K = 2 \times 10^{-7} \text{ m}^{0.1}\text{yr}^{-1}$ , which is then increased to  $1 \times 10^{-6} \text{ m}^{0.1}\text{yr}^{-1}$ . To perturb uniform rock uplift rate, the initial condition is a river profile equilibrated to uniform erodibility of  $1 \times 10^{-6} \text{ m}^{0.1}\text{yr}^{-1}$  and uniform rock uplift rate of  $250 \text{ mMyr}^{-1}$ , which is then decreased to  $50 \text{ mMyr}^{-1}$ . The step increase in erodibility (or decrease in rock uplift) decreases the new equilibrium steepness such that the upper reaches are brought farther above equilibrium as compared to the lower reaches that remain closer to equilibrium (Fig. 2b middle row). Post-perturbation, channel steepness is greater than that required to balance the background rock uplift rate and the river begins to incise more rapidly than the rock uplift rate (Fig. 2b upper and middle row). The imbalance between uplift and incision allows the river profile to decrease in elevation until the river profile is brought back down to an equilibrium grade, which occurs first at the outlet. This results in a positive-curvature slope-break knickpoint that originates at the outlet and propagates upstream through the river network in a wave-like manner. The knickpoint separates downstream reaches that have achieved the new lower equilibrium steepness from the upstream reaches that retain the original higher steepness. As the transient progresses, a distinct pattern of incision depth emerges, the magnitude of which is everywhere greater than the total rock uplift accumulated during the simulation, with the exception of that at the outlet. Incision depth increases away from the mountain front up until the location of the knickpoint, but then remains uniform upstream due to the uniform steepness, and hence uniform incision rate. Again, the knickpoint within the tributaries and the mainstem collapse to a common  $\chi$  value as expected from them starting at a common point of origin (Fig. 2b middle row). If  $n = 2/3$  or  $5/3$ , the first-order fluvial response is similar to the case in which  $n = 1$ , except knickpoint celerity is reduced or accelerated, respectively (Figs. S1 and S2). A step decrease in erodibility or step increase in uplift rate

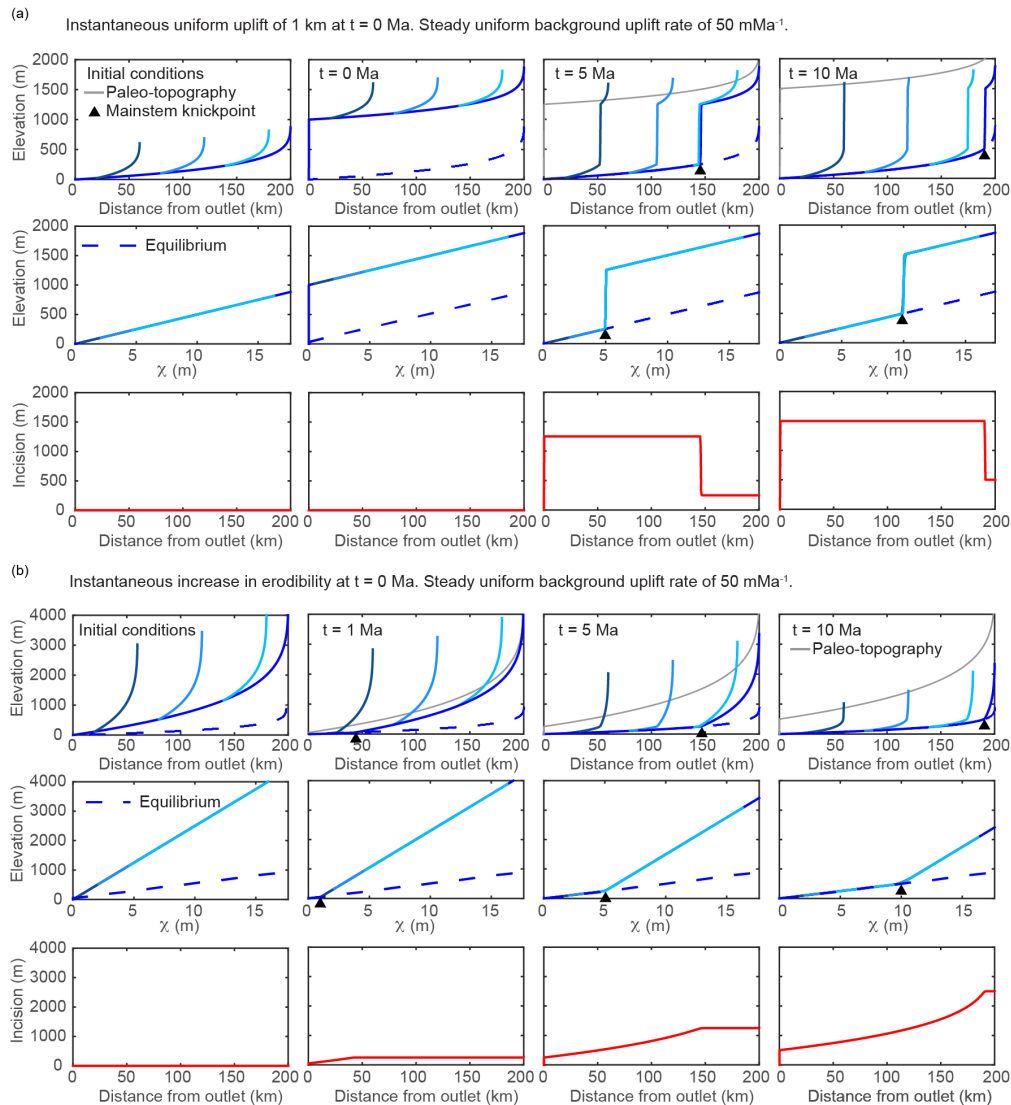


**Figure 2.** Results from 1-D simulations of a river network equilibrated to a uniform background uplift rate of  $50 \text{ mMa}^{-1}$  and subject to various perturbations that move profiles away from equilibrium, but maintain uniform steepness upstream of the propagating knickpoint. (a) Results from multiple timesteps for simulation of instantaneous uniform uplift of 1 km at  $t = 0 \text{ Ma}$  versus (b) a step increase in erodibility,  $K$ , or equivalently a step decrease in rock uplift rate. In (a) and (b), the upper row of plots shows longitudinal profiles with shades of blue corresponding to mainstem and tributaries shown in Fig. 1a. The grey line tracks the pre-perturbation elevation of the river or the potential elevation of paleoriver deposits, i.e. “paleo-topography”. The middle row shows  $\chi$ -elevation profiles ( $\chi$  plots) for the mainstem and tributaries with shades of blue corresponding to mainstem and tributaries shown in Fig. 1a, and the lower row shows incision below the “paleo-topography” markers since  $t = 0 \text{ Ma}$ . In all plots the dashed blue line denotes the final equilibrium state post-perturbation.



produces the inverse of these signatures, with a negative-curvature slope-break knickpoint separating a downstream section that has achieved the new higher equilibrium steepness and an upstream section with uniform, lower steepness (Fig. S3). However, response times are greater in the case in which  $K$  is decreased compared the case in which  $U$  is increased. In both cases, incision depth is greatest at the outlet and is everywhere less than the magnitude of accumulated uplift, except at the outlet.

#### 5 4.3 Truncation of mainstem

The transient response to truncation or beheading of a river network is illustrated in Figure 3a. To simulate truncation, a 100 km section of river profile is removed from the headwaters of a 300 km long river profile equilibrated to a background uplift rate of  $50 \text{ mMyr}^{-1}$  and an erodibility of  $1 \times 10^{-6} \text{ m}^{0.1} \text{ yr}^{-1}$  (Fig. 3a upper row). Channel steepness of the truncated mainstem river profile is everywhere less than that required to balance the background uplift rate and the river profile begins to increase in elevation and steepness (Fig. 3a upper and middle row). Owing to the larger fractional decrease in drainage area in the upper reaches, truncation brings the upper reaches farther below equilibrium than the lower reaches, resulting in negative curvature of the mainstem  $\chi$  plot. Thus, a uniform background rock uplift rate combined with a nonuniform erosion rate mirroring the channel steepness results in a nonuniform surface uplift rate that brings the truncated mainstem river profile back to an equilibrium steepness in a wave-like manner that progresses upstream from the outlet. The tributaries retain the original equilibrium steepness, having not lost drainage area, but are pulled below equilibrium by the area perturbation on the mainstem. Paleotopography markers delineate the location of the original 300 km river that uplifts uniformly with the background uplift rate (Fig. 3a upper row). Only at the channel outlet, where equilibrium channel steepness was retained, does incision reflect rock uplift accumulated from the background uplift rate over the course of the simulation. Upstream of the outlet, incision below paleotopography markers tapers nonlinearly towards zero at the channel head (Fig. 3a lower row). If  $n = 2/3$  or  $5/3$ , the first-order fluvial response is similar to the case in which  $n = 1$ , except knickpoint celerity is reduced or accelerated, respectively.

#### 4.4 Rapid pulse of nonuniform rock uplift due to forward tilting

The transient response to an instantaneous rigid-block tilt about a horizontal axis perpendicular to the mainstem river and located at the river outlet that increases the headwater surface elevation by 1 km with respect to the outlet (tilt of  $\sim 0.3^\circ$ ) is illustrated in Figure 3b. The rapid nonuniform rock uplift rate brings the upper reaches farther above equilibrium as compared to the lower reaches, which remain closer to equilibrium (Fig. 3b upper and middle row). Post tilt, the entire mainstem that drains perpendicular to the tilt axis experiences a uniform increase in profile gradient (equal to the tilt angle), but owing to the nonlinear downstream increase in drainage area, profile steepness,  $k_{sn}$ , is increased by a greater degree near the outlet, resulting in negative curvature of the mainstem  $\chi$  plot. In contrast, the tributaries that drain parallel to the tilt axis are uplifted a uniform amount equal to the rock uplift at each respective tributary junction and are thus offset above equilibrium, but their steepness is not affected (just as described above for uniform uplift). Together, these tilt-induced perturbations to profile steepness and elevation give the  $\chi$  plot of a river network tilted toward the mainstem outlet a unique signature with all portions of the network

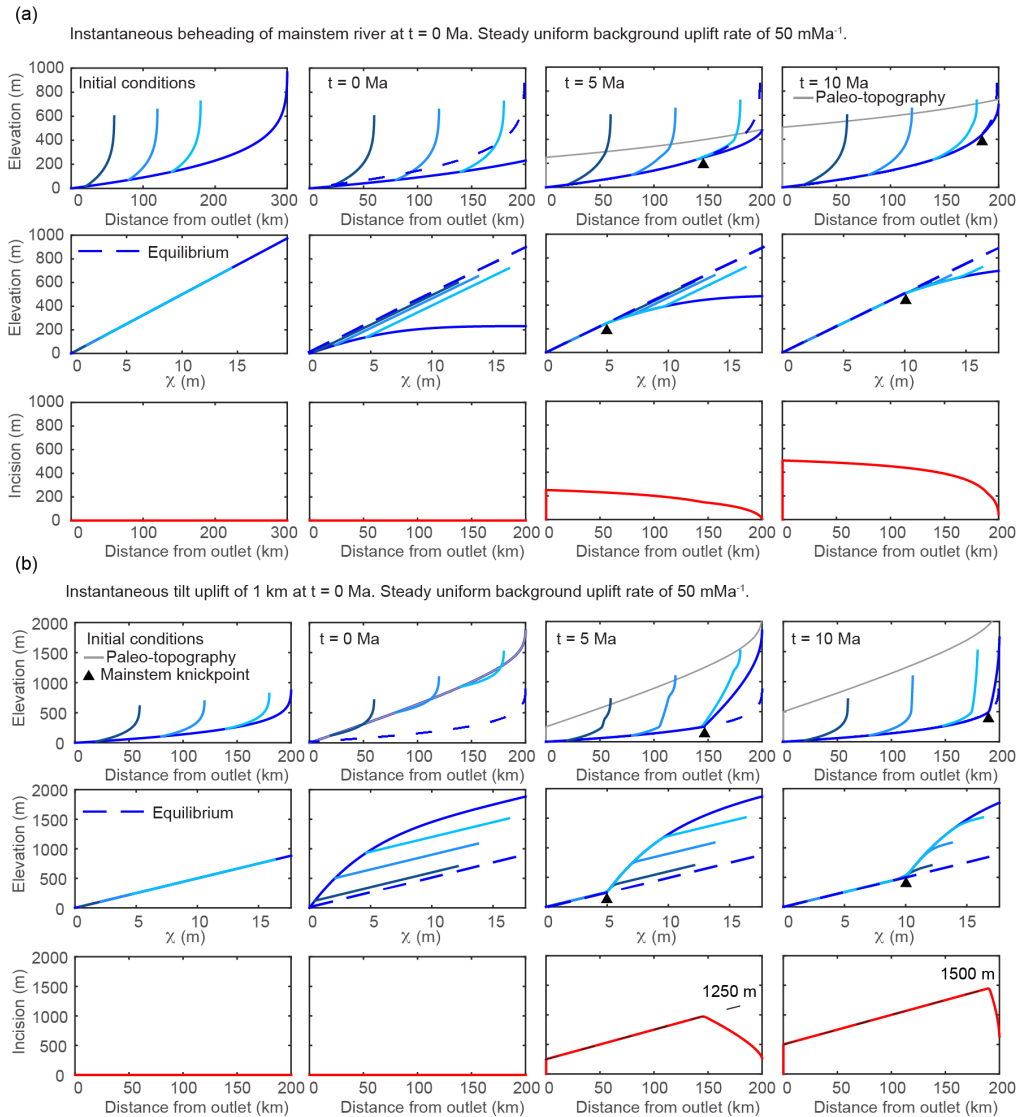


**Figure 3.** Results from 1-D simulations of a river network equilibrated to a uniform background uplift rate of  $50 \text{ mMyr}^{-1}$  and subject to various perturbations that move profiles away from equilibrium and induce nonuniform steepness upstream of the propagating knickpoint. Results from multiple timesteps for simulation of (a) instantaneous truncation of a 300 km long river to a 200 km long river and (b) instantaneous tilting at  $t = 0$  Ma with tilt axis at the river mouth, perpendicular to the main stem, and 1 km maximum uplift at the channel head. Line color, basic description of plots filling each row, and network structure are the same as described in Fig. 2.

plotting above the equilibrium line, but with the mainstem having negative curvature and plotting above uniform steepness (straight) tributaries (Fig. 3b middle row).



After tilting, channel steepness along the entire mainstem is greater than that required to balance the background rock uplift rate and all points on the mainstem begin to incise. The imbalance between uplift and incision allows the mainstem river profile to decrease in elevation until it is brought back down to the pre-tilt equilibrium grade, which occurs first at the outlet owing to the greater steepness and proximity to equilibrium. This results in a positive-curvature slope-break knickpoint that originates at the outlet and propagates upstream through the river network in a wave-like manner. The knickpoint separates a downstream section that has returned to the original pre-tilt equilibrium steepness from an upstream section that is over-steepened and retains the nonuniform tilt-induced steepness that plots as a profile with negative curvature on a  $\chi$  plot. If  $n = 2/3$ , the first-order fluvial response is similar to the case in which  $n = 1$ , except knickpoint celerity is reduced (Fig. S4). If  $n = 5/3$ , knickpoint celerity is accelerated, but the characteristic negative curvature of the mainstem and tributary knickzones can actually become positive with time because of increasing celerity with increasing slope (Fig. S5).

#### 4.4.1 Tributary knickzones record tilt timing

As the over-steepened mainstem incises back to equilibrium, knickzones form at the outlets of tributaries as a response to ongoing base level fall at the junction with the more rapidly incising mainstem. Thus, tributary knickzones begin to form the instant after the tilt perturbation at the outlet of every tributary regardless of position within the basin. The timing of tilt is recoverable from the tributary knickzones by subtracting the  $\tau$  value at the corresponding tributary confluence from the  $\tau$  value at the upstream end of the tributary knickzone. These knickzones are unique in that they are neither vertical-step knickpoints nor are they slope-break knickpoints. Rather, the base of the knickzone is marked by a slope-break knickpoint but upstream of this point they have significant length along which steepness is nonuniform and equal to that of the mainstem upstream of the tributary junction. This results in a perfect collapse of tributary knickzones with the mainstem on  $\chi$  plots.

#### 4.4.2 Tributary knickzone drop height and incision depth reflect tilt magnitude

Tributary knickzones reach their maximum height when the mainstem slope-break knickpoint is at the tributary junction. They then propagate upstream at this maximum height and leave an equilibrium grade tributary profile in their wake. Tributary knickzone height increases linearly moving up the mainstem at a rate equal to the tilt angle up to the mainstem slope-break knickpoint and then decreases moving further upstream. Below the mainstem knickpoint, tributary knickzone height is equal to the local rock uplift from the pulse of tilting, which is equal to the surface uplift following the perturbation, whereas incision depth below the uplifted initial profile (Fig. 3b lower row) is equal to the total rock uplift accumulated since the beginning of the simulation (background rate plus tilting pulse). At intermediate times steps in the transient evolution, a distinct triangular pattern of incision depth below paleotopography markers is evident (Fig. 3b lower row). Incision depth increases linearly with distance from the mountain front with the location of maximum incision corresponding to the slope-break knickpoint in the mainstem, above which incision depth rapidly decreases owing to the upstream decrease in steepness. The linear increase in incision depth with distance from the outlet reflects the linear rock uplift gradient due to tilting and projection of this gradient of incision depth to the channel head accurately recovers channel head surface uplift resulting from tilting plus uplift accumulated from the uniform background rate (Fig. 3b lower row).



#### 4.5 Rapid pulse of nonuniform rock uplift due to back tilting

The transient response to an instantaneous rigid-block tilt about a horizontal axis perpendicular to the mainstem river and located at the channel head that increases the outlet surface elevation by 200 m with respect to the channel head (tilt of  $\sim 0.06^\circ$ ) is illustrated in Figure S6. The response is similar to the transient response to forward tilting in that tilting induces a mainstem knickpoint, nonuniform steepness in the mainstem, and distinct patterns in tributary steepness over which tributaries collapse with the mainstem on the  $\chi$  plot. However, many of the specific characteristics of these signatures are reversed when the uplift gradient relative to the mainstem flow direction is reversed in the back-tilted case (compare Fig. 3b with Fig. S6). Post-tilt, the lower reaches are brought farther above equilibrium compared to the upper reaches and, although the entire mainstem experiences a uniform decrease in gradient,  $k_{sn}$  is decreased by a greater degree near the outlet owing to the nonlinear downstream increase in drainage area, resulting in positive curvature of the mainstem  $\chi$  plot. Similar to the response to forward tilting, the tributaries that drain parallel to the tilt axis are uplifted a uniform amount equal to the rock uplift at each respective tributary junction and are thus offset above equilibrium, but their steepness is not affected. However, in the back-tilted case tributaries are farther above equilibrium than the mainstem and plot above the mainstem in the  $\chi$  plot.

The primary difference in the transient response to back-tilting as compared to forward-tilting is the character of the mainstem knickpoint. Back-tilting induces a vertical-step knickpoint, rather than a slope-break knickpoint, owing to uplift of the river outlet. The vertical-step knickpoint retains its original height as it propagates upstream, briefly raising mainstem elevation until the knickpoint passes and mainstem elevation returns to equilibrium. The vertical-step knickpoint propagates up tributaries, with tributaries collapsing with the mainstem on the  $\chi$  plot over the vertical-step, similar to the transient response to a uniform pulse of uplift. The drop height of the vertical-step knickpoint thus only reflects the magnitude of the pulse of rock uplift at the river outlet. Although the mainstem temporarily rises during the transient response, the entire landscape has not experienced equivalent surface uplift. The location of the vertical-step knickpoint records the timing of perturbation in both the mainstem and tributaries. The transient mainstem response also inscribes a distinct incision pattern in which incision decreases linearly upstream up to the mainstem knickpoint where a sharp decrease is followed by increasing incision upstream. Incision downstream of the vertical-step knickpoint records total accumulated rock uplift post-tilt, that is, the sum of uplift from the punctuated tilt and uplift accumulated from the background uplift rate during the transient response.

Mainstem steepness upstream of the knickpoint is less than equilibrium steepness owing to the initial back-tilting. As a result of the reduced steepness, mainstem erosion does not keep pace with uplift rate. The tributaries experience this as ongoing base level rise from the time of rapid tilting until the mainstem knickpoint passes the tributary junction. The ongoing base level rise induces low-gradient reaches in the tributaries that collapse with the mainstem, analogous to the tributary knickzones formed in the forward-tilting case as a result of ongoing lowering of tributary base level. These low-gradient reaches record tilt timing in the position of the upstream end relative to tributary junction, in the same manner that tributary knickzones record timing in the forward-tilting case. Unlike the forward-tilting case, tributary knickzones do not record the magnitude of rock uplift.



#### 4.6 Rapid pulse of nonuniform rock uplift due to side tilting

The transient response to an instantaneous rigid-block tilt about a horizontal axis parallel to the mainstem river and located along the mainstem that increases the tributary channel head surface elevation by 400 m (tilt of  $\sim 0.3^\circ$ ) is illustrated in Figure S7. For this simulation, we used a slightly different model network configuration in which the three tributaries all joined the mainstem on the uplifted side. The response is identical to that of forward tilting except in this case the mainstem remains at equilibrium and the tributaries are steepened. Analogous to the mainstem in the forward-tilting case, all tributaries have negative curvature on the  $\chi$  plot, positive-curvature mainstem knickpoints, and incision patterns that increase upstream up to the mainstem knickpoints and decrease upstream (Fig. S7).

#### 4.7 Rapid pulse of nonuniform rock uplift due to forward tilting with heterogeneous lithology

We ran two simulations to explore lithologic effects on transient river profiles resulting from nonuniform uplift: 1) a 1 km instantaneous forward tilt of a 200 km long equilibrium river with a 50 km wide vertical bed of rock with anomalously high erodibility from 70 – 120 km upstream (Fig. 4a), and 2) a 1 km instantaneous forward tilt of a 200 km long equilibrium river with a 20 km wide vertical bed of rock with anomalously low erodibility from 30 – 50 km upstream (Fig. 4b). We used  $K = 1 \times 10^{-6} \text{ m}^{0.1}\text{yr}^{-1}$  for the majority of the 1-D river and the tributaries,  $K = 1 \times 10^{-5} \text{ m}^{0.1}\text{yr}^{-1}$  for the vertical bed of more erodible rock, and  $K = 2 \times 10^{-7} \text{ m}^{0.1}\text{yr}^{-1}$  for the vertical bed of less erodible rock.

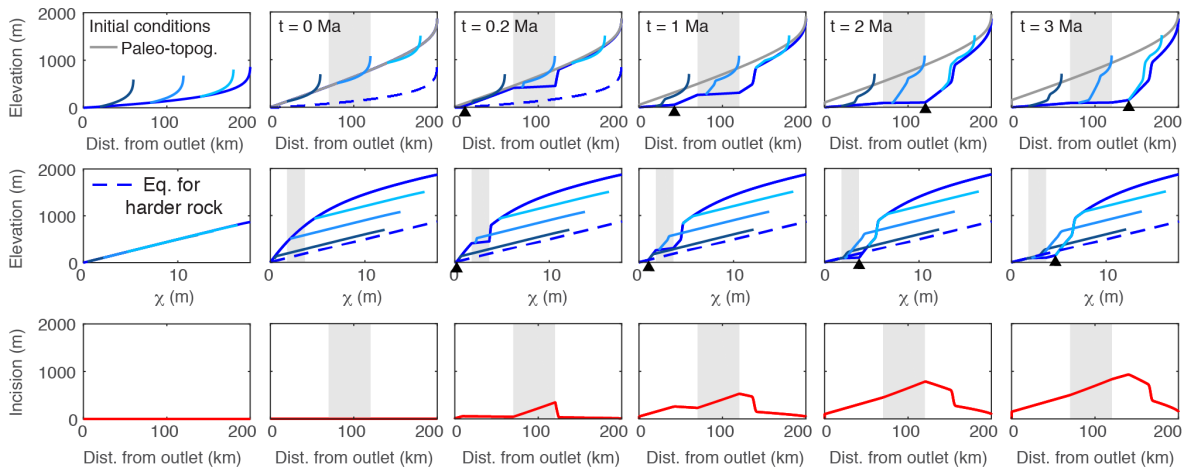
The transient responses observed in these simulations are similar to the one described above in section 4.4 in that a positive-curvature slope-break knickpoint forms at the outlet of the mainstem and propagates upstream, hereafter referred to as the “main slope-break knickpoint”. However, in the tilting simulations with heterogeneous lithology, additional positive-curvature slope-break knickpoints form at the downstream end of the vertical bed of more erodible rock (Fig. 4a) and the upstream end of the vertical bed of less erodible rock (Fig. 4b), hereafter referred to as “rock-type slope-break knickpoints”. As these additional knickpoints propagate upstream, they have a similar effect on tributary profiles and incision depth as the main slope-break knickpoint in that they generate the same unique tributary knickzones and a triangular pattern of increasing incision depth upstream.

The important distinction between the main slope-break knickpoint and the rock-type slope-break knickpoints is that rock-type slope-break knickpoints can form immediately following tilting anywhere along the river profile where more erodible rock occurs upstream of less erodible rock. This can result in localized deviations to the pattern in tributary knickzone height described above. In both simulations with heterogeneous lithology, large tributary knickzones and local maxima of incision depth occur upstream of the main slope-break knickpoint where propagating rock-type knickpoints have lowered the mainstem.

In the high-erodibility simulation, the rock-type slope-break knickpoint that forms at the downstream end of the vertical bed of more erodible rock rapidly propagates upstream owing to greater celerity in the more erodible rock (Fig. 4a). In the wake of the rock-type knickpoint a reach of quasi-equilibrium steepness is formed. The quasi-equilibrium steepness is equilibrated to the rate of baselevel fall at the downstream end of the vertical bed of more erodible rock, which during the transient is higher than the background rate of rock uplift. Thus the quasi-equilibrium steepness is steeper than the final equilibrium steepness,



(a) Instantaneous tilt uplift of 1 km at  $t = 0$  Ma with band of more erodible rock at 70-120 km upstream. Steady uniform background uplift rate of  $50 \text{ mMa}^{-1}$ .



(b) Instantaneous tilt uplift of 1 km at  $t = 0$  Ma with band of less erodible rock at 30-50 km upstream. Steady uniform background uplift rate of  $50 \text{ mMa}^{-1}$ .

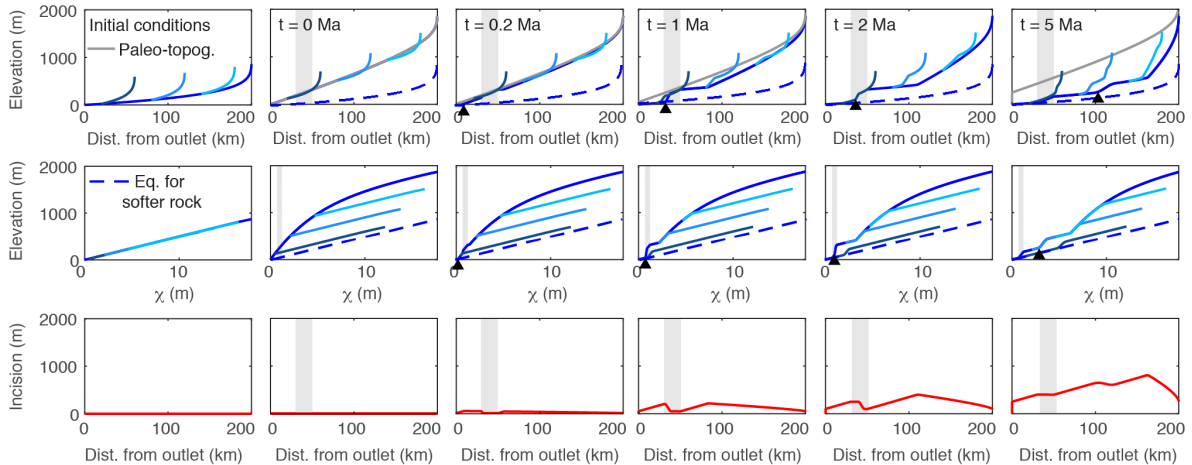


**Figure 4.** Results from a 1-D simulation of an equilibrated river network subject to instantaneous tilting of 1 km at the channel head with (a) a band of more erodible rock at 70-120 km upstream and (b) a band of less erodible rock at 30-50 km upstream. Line color, basic description of plots filling each row, and network structure are the same as described in Fig. 2. In both (a) and (b),  $K = 1 \times 10^{-6} \text{ m}^{0.1} \text{ yr}^{-1}$  was used for the majority of the river profile aside from a 50 km vertical band (shown in grey) which was assigned a  $K$  value of  $1 \times 10^{-5} \text{ m}^{0.1} \text{ yr}^{-1}$  in (a) and a 20 km band (shown in grey) which was assigned a  $K$  value of  $2 \times 10^{-7} \text{ m}^{0.1} \text{ yr}^{-1}$  in (b). In (a), the band of more erodible rock (shown in grey) has  $K = 1 \times 10^{-5} \text{ m}^{0.1} \text{ yr}^{-1}$  whereas  $K = 1 \times 10^{-6} \text{ m}^{0.1} \text{ yr}^{-1}$  was used for the rest of the river profile. In (b), the band of less erodible rock has  $K = 2 \times 10^{-7} \text{ m}^{0.1} \text{ yr}^{-1}$  whereas  $K = 1 \times 10^{-6} \text{ m}^{0.1} \text{ yr}^{-1}$  was used for the rest of the river profile.

but is much less than that found immediately post-tilt, which combined with the rapid response in the more erodible bed



generates a knickzone upstream of the rock-type slope-break knickpoint. At very early times in the simulation ( $t = 0.2$  Ma) large changes in steepness correspond perfectly to lithologic boundaries. Even at  $t = 2$  Ma a large increase in steepness occurs at the upstream contact. However, once the main slope-break knickpoint has propagated past the vertical bed of erodible rock, changes in equilibrium steepness at the lithologic boundaries are much more subtle than those displayed during the transient evolution (Fig. 4a upper row,  $t = 3$  Ma).

In the low-erodibility simulation, the vertical bed of less erodible rock impedes the propagation of the main slope-break knickpoint and an additional rock-type knickpoint forms at the upstream end of the vertical bed of more erodible rock (Fig. 4b). As the main slope-break knickpoint propagates slowly through the vertical bed of less erodible rock, channel steepness is elevated within the less erodible vertical bed for many time steps. While the main knickpoint is held up in the less erodible rocks, the upstream rock-type knickpoint is not impeded and moves much more rapidly upstream and leaves a profile with quasi-equilibrium steepness in its wake. Similar patterns in both incision and tributary knickzone drop height emerge upstream of the vertical bed of less erodible rock as in the tilting simulation with uniform  $K$ . However, within the low-erodibility vertical bed and in particular at the upstream end of the vertical bed, little incision occurs, which results in a local minima in incision depth and tributaries with junctions within the vertical bed that do not exhibit knickzones until the main knickzone propagates through (Fig. 4b upper and lower row). Once the main knickpoint has propagated through the vertical bed of less erodible rock, the changes in equilibrium channel steepness at the lithologic boundaries are much less prominent than those displayed during the transient evolution.

#### 4.7.1 Effects of heterogeneous lithology on $\chi$ plots

In both the high-erodibility and low-erodibility simulations, only tributaries with the same path integral of rock type as the mainstem collapse with the mainstem in the  $\chi$  plot, in contrast to the simulation of tilting with uniform erodibility in which all tributaries collapse with the mainstem. We calculated  $\chi$  with the incorrect assumption of uniform  $K$  and, as  $\chi$  is an integral quantity calculated in the upstream direction, this leads to incorrect  $\chi$  values not just within the vertical beds of anomalous erodibility, but for the entire profile upstream. Although we could easily calculate  $\chi$  with the correct value of  $K$  included in the integral, we chose not to in order to illustrate the effects that even small bands of heterogeneous lithology can have on  $\chi$  plots when changes in  $K$  are unaccounted for. In the high-erodibility simulation,  $\chi$  values are incorrectly high for the mainstem and tributaries upstream of the vertical bed of more erodible rock and these profiles will thus plot below the equilibrium line that does not account for the more erodible rock (Fig. 4a middle row and Fig. 5). In the low-erodibility simulation,  $\chi$  is incorrectly low for the mainstem and tributaries upstream of the vertical bed of less erodible rock and these will thus plot above the equilibrium line that does not account for the low-erodibility rock (Fig. 4b middle row and Fig. 5).

#### 4.7.2 Estimating tilt magnitude from rock-type knickzone geometry in profiles with heterogeneous lithology

At early time steps in the simulation of instantaneous tilting with a vertical bed of more erodible rock, the river profile has a deeply incised section that appears as a triangular "bite" out of the tilted river profile where the river crosses the more erodible

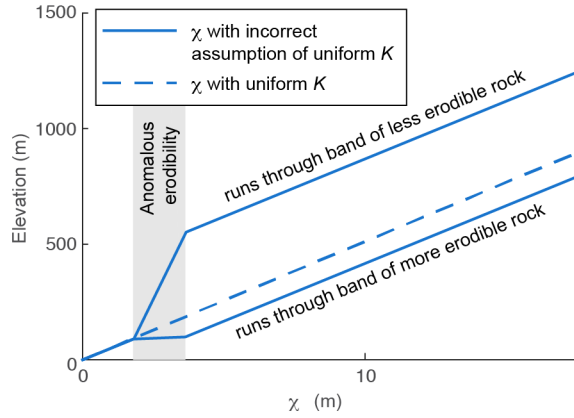


**Figure 5.** Influence of unaccounted for vertical bed of more or less erodible rock on equilibrium  $\chi$  plots for a 200 km river. Dashed  $\chi$ -z profile has a uniform  $K$  of  $1 \times 10^{-6} \text{ m}^{0.1}\text{yr}^{-1}$ . The lower solid profile has a vertical bed of more erodible rock with  $K = 1 \times 10^{-5} \text{ m}^{0.1}\text{yr}^{-1}$  at 60 – 110 km upstream as compared to upper solid profile that has a vertical bed of less erodible rock with  $K = 2 \times 10^{-7} \text{ m}^{0.1}\text{yr}^{-1}$  at 60 – 110 km upstream but both were calculated assuming  $K$  is uniformly  $1 \times 10^{-6} \text{ m}^{0.1}\text{yr}^{-1}$ .

rock. If the slope of the quasi-equilibrium reach (as described in the section above) in the vertical bed of more erodible rock is assumed to equal the pre-tilt river slope over the erodible rock, the geometry of this bite reflects the magnitude of tilt such that:

$$\theta_t = \theta_T - \theta_{qer} \quad (9)$$

$$\theta_T = \arctan\left(\frac{H_T}{L_T}\right) \quad (10)$$

$$5 \quad \theta_{qer} = \arctan\left(\frac{H_{qer}}{L_{band}}\right) \quad (11)$$

$$\theta_{ssr} = \arctan\left(\frac{H_{ssr}}{L_{band}}\right) \quad (12)$$

where  $\theta_t$  is tilt angle,  $\theta_T$  is the angle off horizontal over the bite,  $\theta_{qer}$  is the angle off horizontal over the quasi-equilibrium reach,  $\theta_{ssr}$  is the angle off horizontal of the initial steady-state river profile,  $H_T$  is the total elevation drop over the bite,  $H_{qer}$  is the elevation drop over the quasi-equilibrium reach in the band,  $H_{ssr}$  is the elevation drop of the initial steady-state river over the band,  $L_T$  is the total length of river along the bite, and  $L_{band}$  is the length of river through the band (Fig. 6).

To test whether tilt magnitude could be extracted from the geometry of these mid-profile rock-type knickzones, we ran ten simulations with vertical beds of rock with  $K = 1 \times 10^{-5} \text{ m}^{0.1}\text{yr}^{-1}$  of varying length in which we tilted the same initial



equilibrium profile by the same tilt magnitude. We ran simulations with low background uplift rate ( $U = 50 \text{ mMyr}^{-1}$ ) to achieve a low gradient initial river slope to then tilt  $0.5^\circ$  (Fig. 6b) and a high background uplift rate ( $U = 200 \text{ mMyr}^{-1}$ ) to achieve a high gradient initial river slope subject to then tilt  $0.5^\circ$  (Fig. 6c). In all simulations the initial profile was equilibrated to the same nonuniform values of  $K$  used in the simulation. We identified the upstream and downstream ends of the rock-type slope-break knickpoint defining the knickzone base by identifying the appropriate peak and trough in profile curvature and stopped the simulation when the knickpoint was at the upstream end of the band and the quasi-equilibrium reach stretched only the full length of the band (e.g., Fig. 6a).

We were able to estimate the tilt angle to within a tenth of a degree using equation 9 by calculating  $\theta_T$  and  $\theta_{qer}$  from measurements of  $H_T$ ,  $L_T$ , and  $H_{qer}$  made at the end of each simulation. Estimates of tilt angle do not vary with band width (Fig. 6b and c). In all simulations, the method underestimates tilt magnitude because the quasi-equilibrium slope is greater than the initial equilibrium river slope through the band owing to the fact that the quasi-equilibrium slope is adjusted to a transient rate of base level fall that is greater than the background rate of rock uplift (e.g., Fig. 6b and c). We were also able to measure tilt angle in simulations using a larger magnitude tilt (Fig. S8a) or a smaller difference in erodibility between the bands, but with greater error (Fig. S8). The error in the tilt estimate increases with increasing tilt magnitude and decreasing erodibility because the gradient of the quasi-equilibrium reach becomes greater than the initial river slope across the erodible band in both of these cases (Fig. S8).

#### 4.8 Rapid pulse of nonuniform rock uplift with alternative initial and final conditions

The geomorphic signatures of the transient response to tilting outlined above apply under the conditions that tilting is the predominant perturbation and that the initial condition is a river profile near equilibrium. These conditions may not be met in real landscapes where multiple perturbations may occur with similar timing or where rivers may not have reached equilibrium prior to tilting. To illustrate which geomorphic signatures of tilt outlined above are most robust, we simulated a rapid pulse of nonuniform uplift due to tilting with different initial conditions and histories of background rock uplift rates.

We simulated an instantaneous tilt of an equilibrium profile with a simultaneous step increase in uniform background rock uplift rate from  $50 \text{ mMyr}^{-1}$  to  $200 \text{ mMyr}^{-1}$  such that final fluvial relief was greater than initial fluvial relief (Fig. S9). The initial condition was a river profile equilibrated to a uniform background uplift rate of  $50 \text{ mMyr}^{-1}$  and an erodibility of  $1 \times 10^{-6} \text{ m}^{0.1}\text{yr}^{-1}$ . The new equilibrium steepness is similar to the maximum steepness of the tilted river profile, obscuring the slope-break knickpoint (Fig. S9). With a larger magnitude step increase in uplift rate, the sign of the slope-break knickpoint would flip from positive to negative. The pattern in channel steepness upstream of the mainstem knickpoint remains a robust signature of a punctuated tilting event despite the step change in uplift rate, with mainstem maximum steepness still occurring just upstream from the knickpoint and the mainstem plotting above the tributaries in the  $\chi$  plot. A simultaneous step change in background uplift rate also affects estimates of surface uplift from the magnitude of incision below paleo-topography markers in that incision depth divided by surface uplift is inversely correlated with fractional change in fluvial relief (Fig. S10). For example, a simultaneous step increase in uniform background rock uplift rate along with tilting results in less incision and therefore a lower estimate of surface uplift.

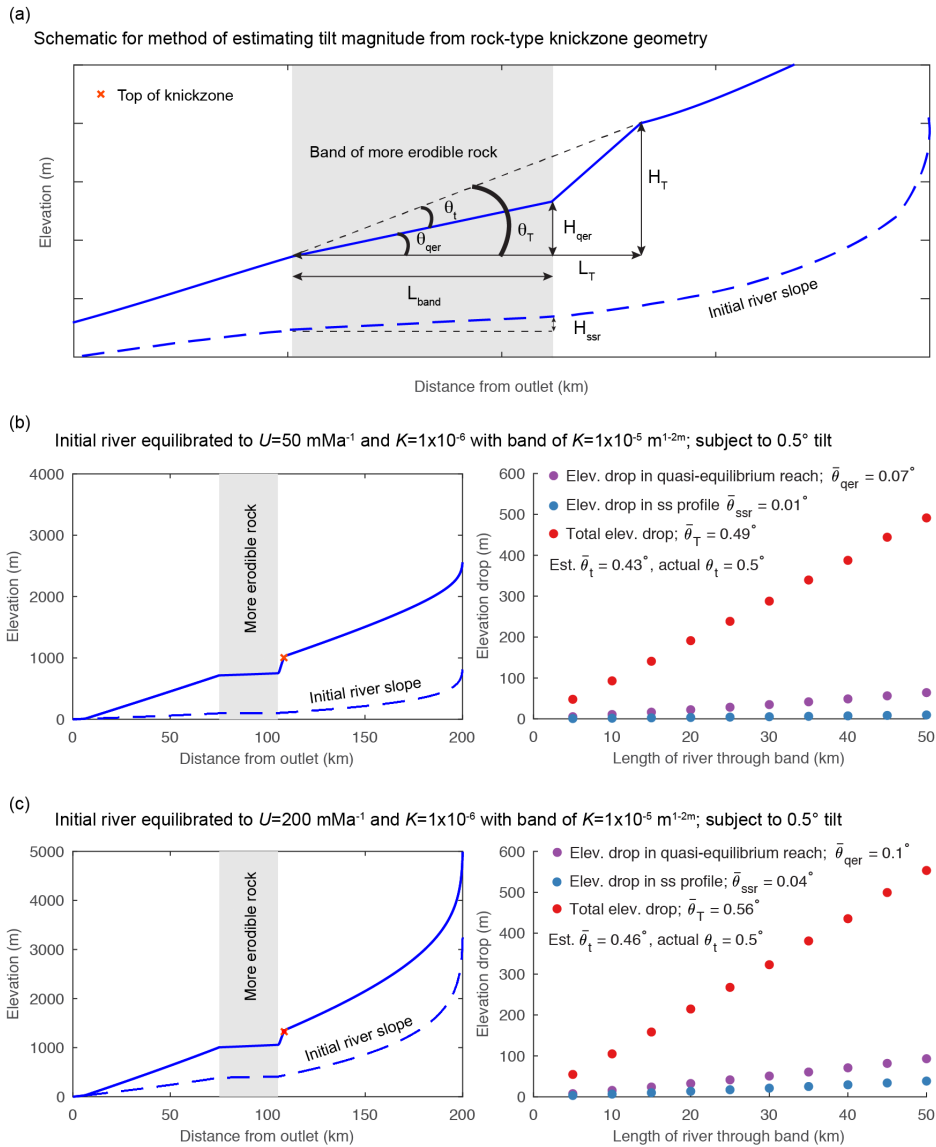


**Figure 6.** Measurements of tilt angle from the geometry of local rock-type related knickzones in a 1-D model of instantaneous forward tilt at  $t = 0$  with vertical beds of more erodible rock of increasing length at 75 km upstream in a 200 km long river. Erodibility in the vertical bed of more erodible rock is 10 times greater ( $K = 1 \times 10^{-5} \text{ m}^{0.1} \text{ yr}^{-1}$ ) than the rest of profile ( $K = 1 \times 10^{-6} \text{ m}^{0.1} \text{ yr}^{-1}$ ) and initial river profile is equilibrated to these nonuniform values of  $K$ . (a) Schematic for variables used in equations 9-12. (b) Example of end time step transient river profile for simulations using low gradient initial river and subject to  $0.5^\circ$  tilt (left) and measurements made from ten simulations with this set up but variable band width (right). (c) Example of end time step transient river profile for simulations using steep initial river and subject to  $0.5^\circ$  tilt (left) and measurements made from ten simulations with this set up but variable band width (right).



To demonstrate how disequilibrium initial conditions affect the geomorphic signatures of tilt, we ran two simulations: 1) a uniform pulse of uplift at  $t = 0$  Ma and an instantaneous tilt of 1 km at the channel head at  $t = 5$  Ma (Fig. S11a), and 2) an instantaneous tilt of 1 km at the channel head at  $t = 0$  Ma and another tilt of the same magnitude at  $t = 5$  Ma (Fig. S11b). Following the second perturbations at  $t = 5$  Ma, the positive-curvature mainstem knickpoint and the pattern in channel steepness upstream of the knickpoint remain robust signatures of tilt that are recognizable in both simulations despite the additional disequilibrium forms in the river profiles. Incision depth in each case reflects the combined surface uplift that has occurred over both perturbations. Thus, the expected pattern emerges from the simulation of two tilting events, but the expected pattern is obscured in the simulation in which the river is first subjected to a uniform pulse of uplift.

## 5 Modeling entire river network response to a rapid pulse of nonuniform rock uplift due to forward tilting

To investigate how landscapes respond to instantaneous tilting beyond the idealized channel network explored above, we used a 2-D numerical landscape evolution model described by Perron et al. (2008) to solve equation 1 and simulate a  $1^\circ$  instantaneous forward tilt of a landscape (down towards the mainstem outlets) equilibrated to an uplift rate of  $50 \text{ mMyr}^{-1}$ , an erodibility coefficient of  $1 \times 10^{-6} \text{ m}^{0.1} \text{ yr}^{-1}$  and river concavity,  $\theta$ , of 0.45, with  $n = 1$  (Fig. 7a). We calculated  $\chi$  for the main river network that drains towards lower boundary and removed all rivers draining to other boundaries from the analysis.  $\chi$  plots for the simulated river network show a similar pattern as the simplified network of linked 1-D profiles described above, with negative curvature in the headwaters, tributaries plotting below the mainstem, and a positive-curvature slope-break knickpoint propagating upstream (Fig. 7b).

### 5.1 Estimating tilt magnitude from azimuth-gradient relationship in stream segments

We measured azimuth,  $k_{sn}$ , and gradient of 3 km long river segments for the entire river network (Fig. 7). We plotted  $k_{sn}$  and gradient against azimuth and calculated running medians for both using a  $10^\circ$  moving window (green line in Fig. 7c and d) to compare to the expected post-tilt signature of a cosine function with a maximum in the tilt direction of  $180^\circ$  (blue line in Fig. 7 d). The distribution of azimuth across all 3 km segments was relatively uniform throughout the simulation (e.g., Fig. 7b inset). Clear signatures of tilt appear immediately after tilting in both the relationships between azimuth and the moving median of  $k_{sn}$  and gradient as stream segments flowing in the direction of tilt ( $180^\circ$ ) have higher gradient and higher  $k_{sn}$ . However, the signature of increased gradient and  $k_{sn}$  in segments flowing in the direction of tilt is much stronger than the signature of decreased gradient and  $k_{sn}$  in segments that were back-tilted (Fig. 7), likely because many back-tilted segments were depressions that were filled during flow routing immediately post-tilt. Both signatures in gradient and  $k_{sn}$  are obscured by the ongoing erosional response by  $t = 4$  Ma and, instead of returning to pre-tilt conditions, median gradient and  $k_{sn}$  are greater at every azimuth at  $t = 4$  Ma (Fig. 7). Unlike the response to uniform uplift, which is dependent on the channel response time, channels respond instantaneously to tilt because steepness has changed everywhere in the river network (Fig. 3b).

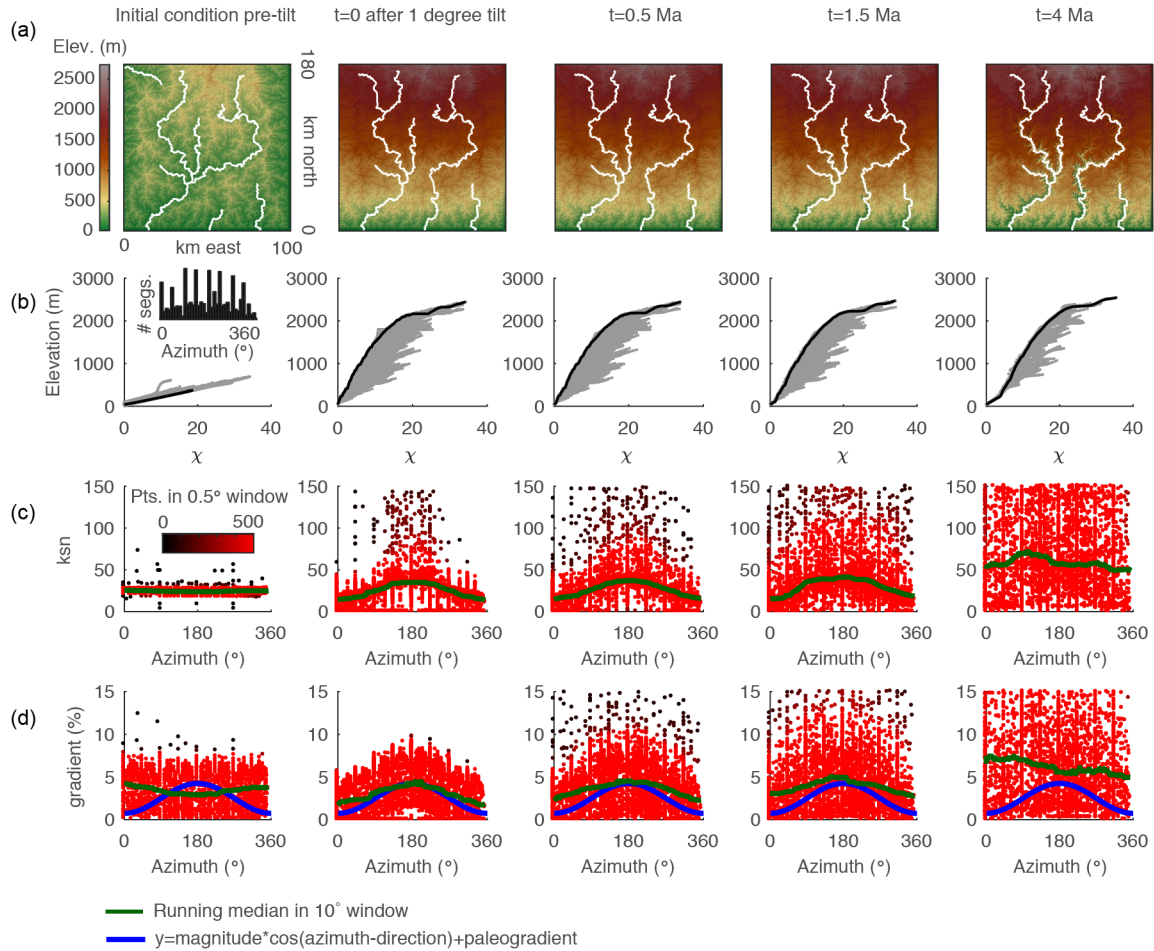


**Figure 7.** Evidence of tilt in relationships between azimuth and gradient and  $k_{sn}$  of 3 km long segments of river networks generated in a 2-D simulation of a  $1^\circ$  instantaneous tilt. **(a)** DEMs with mainstems of the stream network shown in white. **(b)**  $\chi$  plots for entire river network with points on the mainstem shown in black and all tributary points shown in gray. **(c)** Plot of segment  $k_{sn}$  against azimuth with point color indicating density of points within  $0.5^\circ$  azimuth window. **(d)** Plot of segment gradient against azimuth colors as in **c**. Inset in **b** shows the distribution of azimuth of 3 km stream segments demonstrating that the distribution of segments is approximately uniform pre-tilt. Blue line shows cosine function with known parameters of tilt perturbation in the simulation. Green line shows  $10^\circ$  wide moving-window medians.

## 5.2 River network reorganization in response to rapid tilting

Network topologic changes via stream capture oriented in the direction of tilt characterized river network reorganization post tilting. We observed two types of stream captures in the model. The first occurred immediately after tilting as a result of our routing algorithm that filled in closed depressions in back-tilted reaches until an outlet could be found, commonly a low point in the bounding ridge. Although these captures resulted purely from our particular routing algorithm, the analogous natural



processes would be aggradation of sediments in back tilted reaches that eventually raise the bed elevation to the point of spilling over the ridge to complete a stream capture (e.g. Fig. 8b). At later time, the second type of stream capture occurred when knickzones in over-steepened streams flowing in the tilt direction eroded headward and breached ridges separating more rapidly eroding streams in the tilt direction from more slowly-eroding back-tilted reaches or reaches flowing oblique to the tilt direction (e.g., Fig. 8c). At  $t = 4$  Ma, the captured stream network appear as regions with anomalous topology, including barbed tributaries and streams that cut through ridges (Fig. 8c). With a lower tilt magnitude but the same initial condition, the first style of "tilt-and-spill" stream capture becomes less likely, but capture owing to headward migration of over-steepened streams remains as likely.

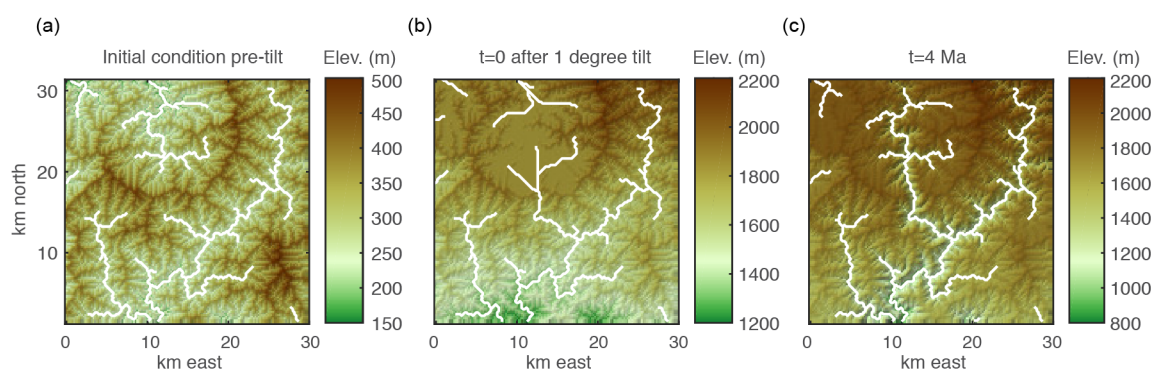


**Figure 8.** Examples of stream capture in the tilt direction from 2-D simulation of a 1 degree instantaneous tilt at  $t = 0$  Ma. Maps show DEMs overlaid with stream network in white for (a) initial condition pre-tilt, (b)  $t = 0$  after  $1^\circ$  tilt, and (c) at  $t = 4$  Ma.

## 6 Example of the geomorphic expression of a punctuated tilting event from the Sierra Nevada, California

10 We analyzed mainstem and tributary profiles of the Middle Fork American River basin, in the northern part of the Sierra Nevada (see Fig. 9 for location), as an example of how the geomorphic signatures of transient response to rapid tilting as outlined above can be used in concert to reconstruct timing and magnitude of a tilting event in a range long thought to have been tilted westward in the late Cenozoic. The Sierra Nevada is a  $\sim 600$  km long  $\sim 100$  km wide range striking northwest-southeast through eastern California (Fig. 9) that is tilted westward  $\sim 0.5 - 1^\circ$  in the northern Sierra (Jones et al., 2004; Lindgren, 1911; Unruh, 1991; Wakabayashi, 2013; Wakabayashi and Sawyer, 2001) and  $\sim 1 - 2^\circ$  in the southern Sierra (Huber, 1981; McPhillips and Brandon, 2012). Although recent geochemical studies suggest the Sierra has been a high topographic feature since the Cretaceous (Cassel et al., 2009; 2012; 2014; Crowley et al., 2008; Hren et al., 2010; Mix et al., 2016; Mulch et al., 2006; 2008; Poage and Chamberlain, 2002), the assumptions inherent in their methods have been questioned (Molnar, 2010), and the majority of studies, including evidence from a range of fields, point to a late Cenozoic pulse of uplift (Christensen, 20 1966; Clark et al., 2005; Ducea and Saleeby, 1996; Huber, 1981; Jones et al., 2004; Lindgren, 1911; McPhillips and Brandon,



2012; Pelletier, 2007; Stock et al., 2004; 2005; Unruh, 1991; Wakabayashi, 2013; Wakabayashi and Sawyer, 2001; Yeend, 1974).

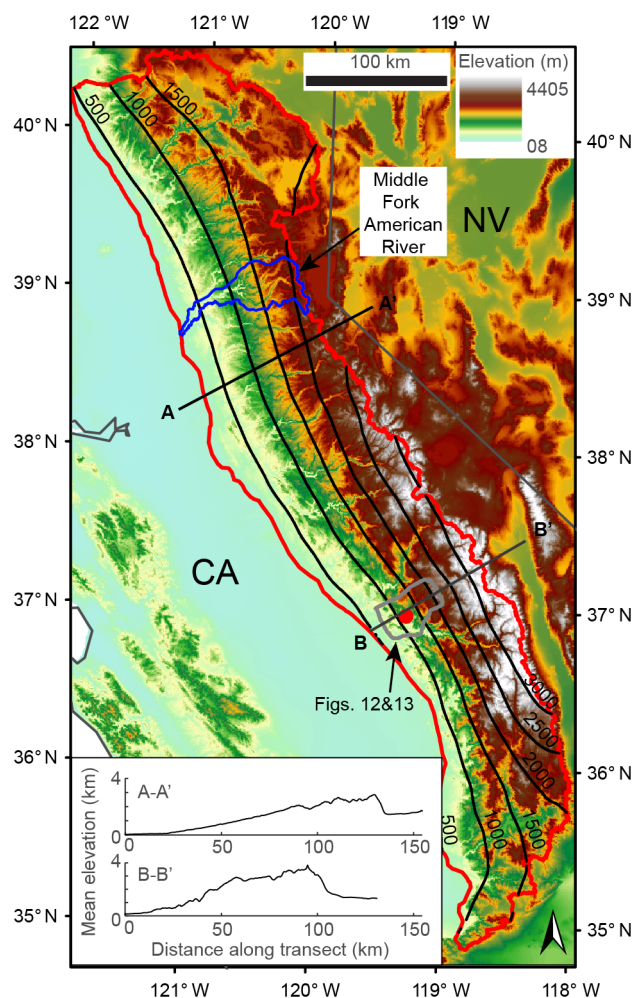


**Figure 9.** Digital elevation model (DEM) of eastern California and western Nevada. The extent of the western slope of the Sierra Nevada is enclosed by a red line with the eastern boundary defining the crest and the western boundary defining the mountain front. The Middle Fork American River basin is enclosed by a blue line, upland interfluve surface analyzed in Fig. 12 is enclosed by a thick grey line, stream capture shown in Fig. 13 is shown with red marker, and 500 m contours of elevation after smoothing DEM with a 50 km<sup>2</sup> moving-window mean are shown with black lines. State lines, shown in grey, of California and Nevada for reference. Inset shows elevation swaths for corresponding transects  $A - A'$  and  $B - B'$ .



## 6.1 Disequilibrium form of the mainstem Middle Fork American consistent with late Cenozoic tilting

A positive-curvature slope-break knickpoint is evident in the mainstem Middle Fork American River at 110 km upstream from the mountain front and 330 m elevation (black triangle in Fig. 10a and b). Downstream of the slope-break knickpoint, channel steepness is low and uniform, whereas upstream of the knickpoint, channel steepness is nonuniform with maximum steepness occurring just above the knickpoint and decreasing upstream. Both the mainstem and the cloud of points defined by the tributaries exhibit negative curvature on the  $\chi$  plot, with the mainstem plotting near the top of the cloud. These disequilibrium profile forms are similar to the signatures of the transient response to forward tilting displayed in the 1- and 2-D simulations outlined above (compare Fig. 10b with Fig. 3b and Fig. 7b).

Using  $\theta = 0.45$ , we calculated that  $k_{sn} = 56$  for the mainstem equilibrium reach below the knickpoint in the Middle Fork American River. Using  $n = 1$  and a river incision rate of  $0.06 \pm 0.01$  mmyr<sup>-1</sup> measured from the Stanislaus River in the northern Sierra from a  $1.63 \pm 0.08$  Ma cave (Stock et al., 2004; 2005) and assuming incision reflects uplift rate, we calculated that  $K \approx 1 \times 10^{-6}$  m<sup>0.1</sup>yr<sup>-1</sup> using equation 5. With  $K = 1 \times 10^{-6}$  and assuming  $K$  is relatively uniform,  $\chi$  values can be interpreted as knickpoint travel times,  $\tau$ , in millions of years (equations 4 and 6). The mainstem slope-break knickpoint occurs at  $\chi = 5$ , thus we estimate that the punctuated tilting event in the northern Sierra occurred *ca.* 5 Ma.

Widespread volcanism blanketed the northern Sierra from the mid-Miocene through the Pliocene (Bateman and Wahrhaftig, 1996; Busby et al., 2008; Christensen, 1966; Curtis, 1953; Durrell 1966; Slemmons 1966). These deposits still blanket modern interfluves throughout the northern Sierra. The depth of incision into the underlying basement rock downstream of the mainstem slope-break knickpoint has been proposed to reflect accumulated rock uplift since their deposition (e.g., Fig. 3b; Wakabayashi, 2013; Wakabayashi and Sawyer, 2001). We measured incision of the mainstem into basement rock below Cenozoic volcanic deposits and plotted it against Euclidean distance from the mountain front (Fig. 10a inset). This revealed that incision depth increases linearly below the mainstem slope-break knickpoint with respect to distance from mountain front as in the simulation of instantaneous tilt (compare Fig. 10a inset with Fig. 3b lower row). By calculating a linear regression of incision data below the mainstem knickpoint as described in section 4.4.2 (Fig. 3b lower row), we estimated a  $0.8^\circ$  tilt or, by projecting this tilt angle the  $\sim 90$  km width of the range,  $\sim 1,200$  m of late Cenozoic surface uplift at the crest (Fig. 10a inset).

Local deviations in the mainstem longitudinal and  $\chi$  profiles as well as the pattern of incision into basement rock may be caused by heterogeneous lithology and/or glacial erosion. At 160 km upstream, the Middle Fork American travels for 9 km through metamorphosed Jurassic marine rocks. This reach has anomalously low channel steepness and occurs downstream of a steep knickzone at the contact with Mesozoic granitic rocks (Fig. 10a). This step exhibits similar characteristics as steps formed in the simulation of instantaneous tilt with a vertical bed of more erodible rock (compare Fig. 10a with Fig. 4a). From the geometry of this knickzone (Fig. 6a and equation 9), we estimated a tilt of  $0.7^\circ$  or  $\sim 1,100$  m of surface uplift at the crest. Such notable profile deviations are not observed in other locations where the river passes through Jurassic marine rocks, likely because bands are downstream of the mainstem slope-break knickpoint where equilibrium changes in steepness across rock types are much more subtle or because this is a grouping of multiple formations (Ludington et al., 2005) and is thus likely comprised of rocks with a range in erodibility.

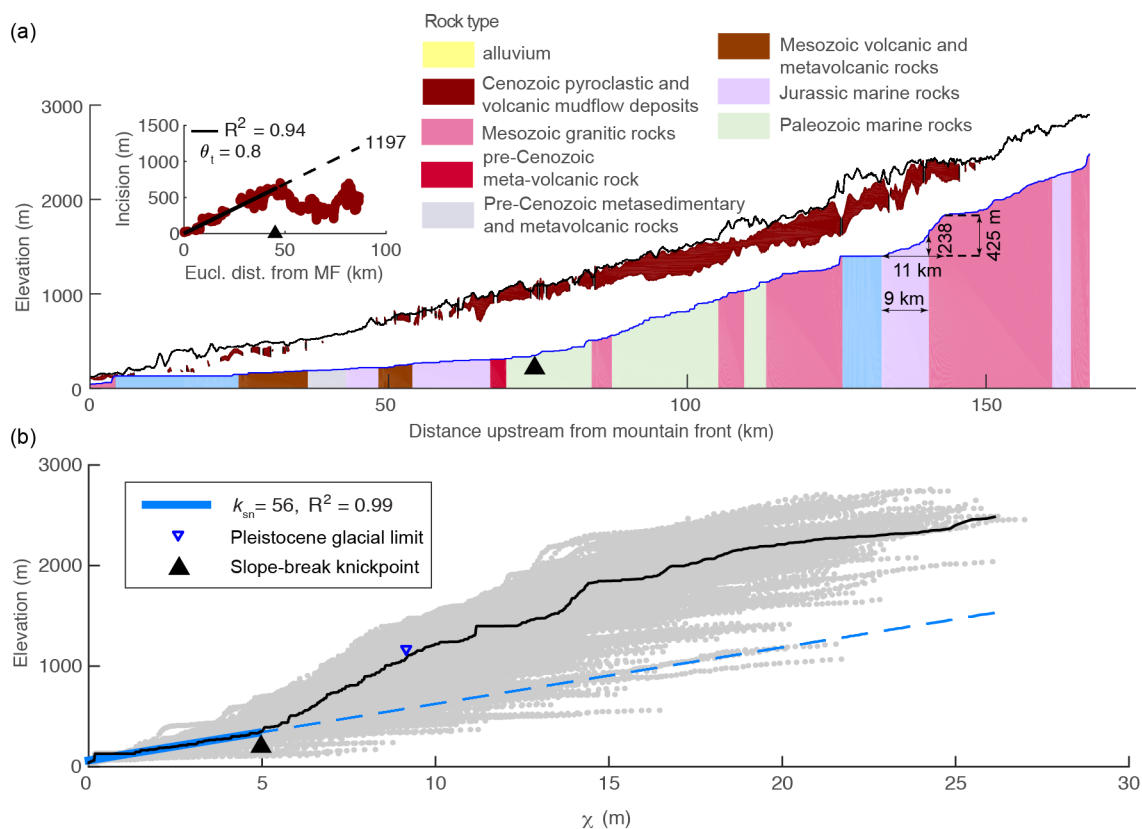


**Figure 10.** Mainstem river profiles for the Middle Fork American River, Sierra Nevada. **(a)** Longitudinal profile (blue line) for mainstem upstream of mountain front, with surface geology fill, ridge topography (black line), Cenozoic volcanic deposits within the basin (brown polygons below black line). Cenozoic volcanic cover was taken from 1:250,000 geology maps (Saucedo and Wagner, 1992; Wagner et al., 1981). Surface geology was taken from 1:500,000 geology maps (Ludington et al., 2005) and was smoothed using a 5 km moving window (i.e., bands of rock <2.5 km river length were removed). Inset plot shows valley incision into basement calculated as the difference between the minimum elevation of proximal Cenozoic volcanic deposits and the modern river profile with a linear regression of data below the mainstem slope-break knickpoint that was projected to the river’s headwaters. **(b)**  $\chi$  plot with mainstem  $\chi$  profile (black) over data from entire basin (grey). Thick blue line highlights data below mainstem slope-break knickpoint that was used in a linear regression that was then projected to the headwaters (dashed blue line).

## 6.2 Middle Fork American tributary knickzones reflect late Cenozoic tilting

We analyzed all major tributaries to the Middle Fork American River and all tributaries have large knickzones between the tributary junction and an upstream section with low channel steepness (Fig. 11). These knickzones have a similar unique character as those formed in the simulation of instantaneous forward tilt, with anomalously high but nonuniform steepness that is similar to that of the mainstem upstream of the tributary confluence (compare Fig. 11 with Fig. 3b). We identified



the upstream end of tributary knickzones visually and measured their drop height as the elevation difference between the upstream end and the confluence with the mainstem. Tributary knickzone drop height increases up to the mainstem slope-break knickpoint and decreases upstream, similar to the pattern generated in the simulation of instantaneous forward tilt (compare Fig. 11 with Fig. 3b).

5 We categorized tributary knickzones as those that collapse with the mainstem on the  $\chi$  plot and thus behave similarly to tributaries in the simulation of instantaneous tilt, and those that do not collapse with the mainstem on the  $\chi$  plot and thus are likely influenced by additional factors that allow the knickzones to move in a manner not captured by the simple stream power law employed here. As described in section 4.4.1, the timing of tilt can be recovered by subtracting the  $\tau$  value at the corresponding tributary confluence from the  $\tau$  value at the upstream end of the knickzone. By using only knickzones that  
10 collapse with the mainstem on the  $\chi$  plot, we estimated the timing of tilt in the Sierra to be *ca.* 1.9 Ma.

We further categorized the tributary knickzones that collapse with the mainstem on the  $\chi$  plot into two groups: those with tributary confluences downstream of the mainstem knickpoint and those with confluences upstream of the knickpoint. The drop height of tributary knickzones that collapse with the mainstem on the  $\chi$  plot and that have junctions downstream of the mainstem slope-break knickpoint should reflect the magnitude of surface uplift as described in section 4.4.2 (e.g., Fig. 3b). By  
15 regressing these points, we estimated  $0.6^\circ$  tilt or  $\sim 950$  m of surface uplift at the crest (Fig. 11 inset).

### 6.3 Tilt magnitude recorded in the stream network on a broad upland interfluvium in the southern Sierra

We located an unglaciated, low-relief surface on the interfluvium between the San Joaquin River and the Kings River in the southern Sierra (full extent of surface shown in Fig. 9 and close-up shown in Fig. 12a). We broke the river network on this surface into 3 km segments and measured azimuth,  $k_{sn}$ , and gradient for all segments just as we had done in the analysis  
20 of the 2-D simulation of instantaneous forward tilt (section 4.7). As with the simulated data, we plotted  $k_{sn}$  and gradient against azimuth and calculated running medians for both using a  $10^\circ$  moving window and observed that gradient values are anomalously high for a  $\sim 180^\circ$  range of azimuth ( $145 - 325^\circ$ ; Fig. 12b and c). By fitting a cosine function to the azimuth-gradient data that fell between  $145 - 325^\circ$  (blue line in Fig. 12c), we estimated a tilt towards  $237^\circ$  (southwest) of magnitude  $2.3^\circ$ , or 3,500 m of surface uplift when projected the  $\sim 90$  km width of the range in this region. We also observed multiple  
25 possible stream captures in the direction of tilt on this interfluvium (e.g., Fig. 13).

## 7 Discussion

A long-standing goal of geomorphology has been to develop tools to extract Earth history from landscape form, but questions remain regarding the degree to which particular perturbations to Earth's surface, whether tectonic or climatic, are recorded in a recognizable manner. In the analysis presented we show that the fluvial response to the simple case of a punctuated rigid-block  
30 tilting event does inscribe identifiable and robust signatures throughout the river network during the transient evolution back towards an equilibrium state. These signatures are composed of unique patterns of channel steepness,  $k_s$ , or gradient normalized for drainage area, in the mainstem as compared to the tributaries and a unique distribution of knickpoints originating at the

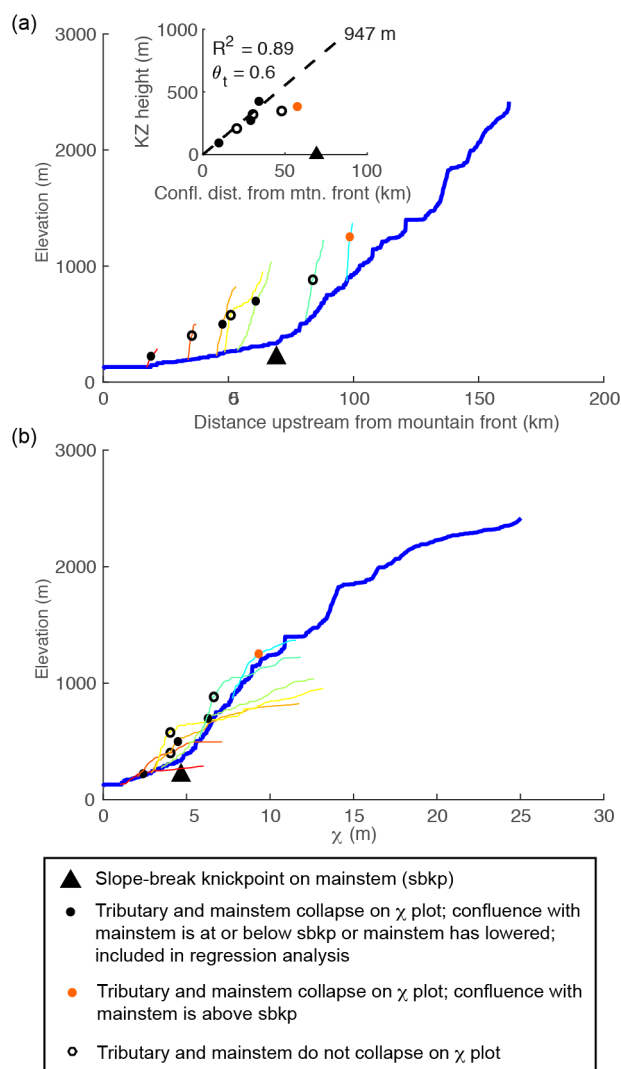


**Figure 11.** Mainstem and tributary profiles for the Middle Fork American River, Sierra Nevada. (a) Longitudinal profiles and (b)  $\chi$  profiles for the mainstem and major tributaries. Mainstem is shown in thicker blue line; tributaries change from warm to cool colors as distance upstream from the mountain front to the tributary confluence increases. Inset plot shows measurements of tributary confluence distance upstream and tributary knickzone drop height along with a linear regression of points with confluences downstream of the mainstem slope-break knickzone whose  $\chi$  profiles collapse with the mainstem through the knickzone.

mainstem outlet and at mainstem-tributary junctions. Tilting about a horizontal axis uniformly increases or decreases the gradient of stream segments perpendicular to the tilt axis, while the gradient of stream segments parallel to the tilt axis remain unchanged by the uniform uplift field parallel to the tilt axis. Owing to the branched nature of river networks, the mainstem river and its tributaries commonly experience very different uplift fields, which, to first-order, is the root cause behind the tilt

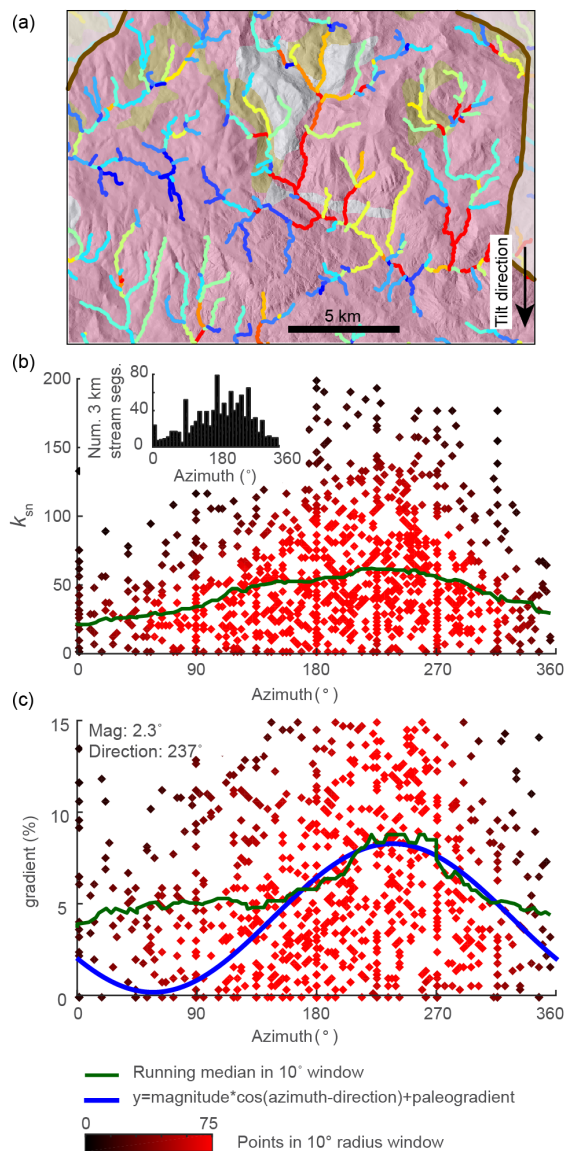


**Figure 12.** Evidence of tilt in relationships between azimuth and gradient and fluvial steepness,  $k_{sn}$ , of the modern river network on a broad upland interfluvial surface between the San Joaquin and Kings Rivers in the Sierra Nevada. (a) Hillshade image colored by geology (colors same as Fig. 10) for a portion of the interfluvial surface overlaid with the stream network colored by  $k_{sn}$  measured over 3 km stream segments. Note higher  $k_{sn}$  in segments flowing in the tilt direction and lower  $k_{sn}$  in segments flowing against the tilt direction. Inset shows a histogram of the azimuth distribution of 3 km stream segments. (b) Azimuth- $k_{sn}$  plot. (c) Azimuth-gradient plot. Green line in (b) and (c) shows 10° wide moving-window median. Blue line in (c) shows the cosine fit which was used to estimate tilt magnitude, the azimuth of tilt direction, and the mean stream gradient pre-tilt (“magnitude”, “direction”, and “paleogradient” in the legend, respectively).

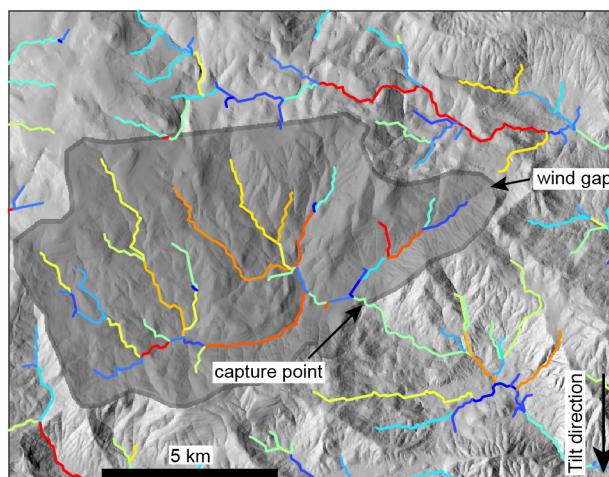


**Figure 13.** Proposed stream capture in the predicted tilt direction in the southern Sierra. Hillshade image with the stream network colored by  $k_{sn}$  measured over 3 km stream segments. Proposed captured area is shaded with dark grey and enclosed by a darker grey line.

signatures described above. Further, the power law relationship between gradient and drainage area that is characteristic of a dendritic river network translates a uniform change in stream gradient to a nonuniform change in  $k_s$ . Analysis of the transient response to tilting clarifies that a uniform increase in channel gradient on the mainstem does indeed generate knickpoints.

To quantitatively investigate the signatures of the transient fluvial response to tilting, we used the detachment-limited stream power model (Howard, 1994; Whipple and Tucker, 1999), which has been shown to produce first-order features of equilibrium and transient bedrock river profile forms as seen in nature (Howard and Kerby, 1983; Siedl and Dietrich, 1992, Tucker and Whipple, 2002, Whipple and Tucker, 1999). We demonstrate that the signatures of tilt are robust and unique by additionally simulating the transient fluvial response to a uniform pulse of uplift and a step change in fluvial relief, both of which have been studied extensively (e.g., Baldwin et al., 2003; Bonnet and Crave, 2003; Grimaud et al., 2016; Howard, 1994; Rosenbloom and Anderson, 1994; Royden and Perron, 2013; Tucker and Whipple, 2002; Whipple and Tucker, 1999), as well as the transient fluvial response to beheading of the mainstem river, the signatures of which have not been thoroughly explored previously. Although we exclusively use the detachment-limited stream power model for the sake of comparing first-order profile forms in the simplest case, the transient response to some perturbations may be more accurately simulated using a transport-limited model. For example, Whipple and Tucker (2002) showed that the transient response to a decrease in uplift rate is eventually accompanied by a transition from detachment-limited to transport-limited conditions. Given the similar declining-state profile form, the transient response to forward tilting may also eventually involve a shift to transport-limited conditions. However, while this may change channel response times and profile forms at later time steps, it is unlikely to significantly change the distinct signatures that characterize first-order profile forms at early time steps. Similarly, perturbations that move mainstem and/or tributary  $k_{sn}$  below equilibrium  $k_{sn}$ , such as mainstem beheading and back tilting, will likely generate an aggrada-



tional response. Future research could exploit the first order signatures of tilting or mainstem beheading as outlined herein to investigate the depositional response and possible transitions to transport-limited conditions.

The detachment-limited stream power model predicts that a punctuated tilting event, similar to other well-explored perturbations (e.g., Baldwin et al., 2003; Tucker and Whipple, 2002; Whipple and Tucker, 1999), will generate a knickpoint in the mainstem that will propagate upstream from the outlet, the location of which will track the timing of the perturbation. In all perturbations explored herein, the mainstem knickpoint separates a downstream section with new, equilibrium  $k_{sn}$  from an upstream section with disequilibrium  $k_{sn}$ , as long as both  $U$  and  $K$  are steady and uniform following the perturbation. Following a uniform pulse of uplift or a step change in fluvial relief, the landscape upstream of the mainstem knickpoint retains the pre-perturbation uniform equilibrium  $k_{sn}$  and is unaffected by the change in boundary conditions until the knickpoint propagates upstream (e.g., Baldwin et al., 2003; Tucker and Whipple, 2002; Whipple and Tucker, 1999).

Unlike a uniform pulse of uplift or a step change in fluvial relief, both rigid-block tilting about a horizontal axis perpendicular to the mainstem and truncation of the mainstem perturb  $k_{sn}$  along the entire mainstem away from an equilibrium state and thus immediately initiate a response along the entire mainstem. In both tilting and truncation, however, the perturbation to  $k_{sn}$  is localized to the mainstem. Following forward tilting, the mainstem is oversteepened and begins to incise, whereas, following back tilting or beheading, the mainstem is everywhere less steep than equilibrium and begins to rise. Immediate, yet transient, mainstem response generates unique patterns in tributary channel steepness that reflect, in the forward-tilting case, a period of transient base level fall that generates a knickzone and, in the back-tilting or beheading case, a period of base level rise that generates a low-gradient reach. In all cases, tributary knickzone  $k_{sn}$  matches that of the mainstem upstream of the tributary junction and hence tributaries collapse with the mainstem on  $\chi$  plots downstream of sections that retain equilibrium  $k_{sn}$ . Similar to how the  $\tau$  value of a mainstem knickpoint tracks the timing of a perturbation (e.g., Whipple and Tucker, 1999), the  $\tau$  value of the upstream end of tributary knickzones can also be used to track timing because  $k_{sn}$  begins to change upon perturbation and the reach with nonuniform  $k_{sn}$  then propagates upstream. In the forward-tilting case, tributary knickzones also record the magnitude of tilt induced rock uplift. In the back-tilting case, tributary knickzone height only reflects the magnitude of rock uplift at the river outlet. Each perturbation explored herein generates a distinct incision pattern as the mainstem river incises below paleotopography markers that records the magnitude of rock uplift in the perturbation plus rock uplift accumulated by the background rate.

In addition to generating robust signatures in river profiles, the transient response to tilting leaves additional distinct signatures in river networks. In a 2-D simulation of instantaneous forward tilt towards river outlets, stream segments flowing in the direction of tilt have increased  $k_{sn}$  and gradient, with the magnitude of tilt recoverable from the relationship between gradient and azimuth in over-steepened reaches, but only shortly after the tilting event. Following forward tilting, gradient and  $k_{sn}$  continue to rise and both remain elevated at all azimuths for millions of years. Tilting can also generate topologic changes oriented in the direction of tilt that can occur coincident with tilting or anytime following tilting while the river network equilibrates. These signatures are unique to nonuniform uplift in that they result from simultaneous nonuniform changes to channel steepness, which in turn generates erosion gradients that allow drainage divides to become mobile throughout the river network.



Through river profile and network analysis in isolated localities in the Sierra Nevada, we showed that proposals for a punctuated tilting event in the late Cenozoic Sierra are consistent with the geomorphic signatures we quantify for a forward tilted landscape. Although our estimates of tilt timing and magnitude made by applying these signatures to the Sierra are consistent with published estimates, variability exists among the suite of independent measures of both timing and magnitude. We present the analysis in the Sierra as an example to show that the geomorphic signatures of the transient response to tilting as outlined herein exist in nature but not as a demonstration of a robust method for characterizing the uplift history of a landscape. For a robust characterization of a landscape's uplift history, river networks across the entire landscape should be analyzed, not isolated profiles as presented here. We present a thorough and systematic analysis of Sierra Nevada river profile and network signatures in a forthcoming paper.

Heterogeneity in real landscapes presents challenges to extrapolating uplift history from landscape form. We demonstrated that deviations in the expected river profile signatures of the transient fluvial response to forward tilting can result from heterogeneous lithology, changes in the stream power slope exponent, disequilibrium initial conditions, or coincident perturbations. During the transient response to forward tilting, knickzones can form anywhere in the river profile where more erodible rock occurs upstream of less erodible rock, with the potential to significantly alter the expected signatures of tilt. Deviations away from  $n = 1$ , which may be associated with a shift in erosional mechanisms (Whipple et al., 2000), would also impact transient profile forms and would additionally affect estimates of timing made from knickpoint locations. Although deviations generated by heterogeneous lithology may be recognized by analyzing profile form with respect to surface geology, and shifts in profile form or relative knickpoint locations could potentially be used to identify changes in erosional mechanisms, constraining initial conditions or teasing apart multiple perturbations presents a major challenge. Tilting generates a suite of signatures that collectively are robust and unique, but individual signatures share characteristics with those produced by other perturbations described herein. Similarly, processes not explored here, such as sediment flux dependent erosion (Lague, 2014; Sklar and Dietrich, 1998; 2004) or changes in channel width with uplift rate (Attal et al., 2011; Finnegan et al., 2005; Lague, 2014; Turowski et al., 2009; Whittaker et al., 2007; Wobus et al., 2006; Yanites and Tucker, 2010; Yanites et al., 2010), may also have the potential to confound signatures of tilt presented here. Thus, it could be difficult to recognize signatures of tilt in river profiles and network patterns if tilting is not the predominant perturbation recorded in landscape form or if erosional mechanisms are nonuniform.

## 8 Conclusions

We investigated the geomorphic signatures of the transient fluvial response to tilting and whether these signatures can be used to quantify uplift histories in terms of timing and magnitude. With a model river network composed of linked 1-D river longitudinal profile evolution models, as well as a full 2-D landscape evolution model, we demonstrated that the transient response to a punctuated tilting event leaves a suite of signatures throughout the river network that are distinct and, in the case of forward tilting towards the river outlet, provide multiple independent measures of tilt timing and magnitude. Further, we show that the signatures of forward tilting are consistent with profile forms and river network patterns observed in the Sierra



Nevada, California, USA, a landscape proposed by many to have experienced a punctuated tilting event in the late Cenozoic. However, we presented only a small sample of the river network draining the west side of the Sierra Nevada. Although the resulting estimates of tilt timing and magnitude are within the range of previous estimates, the variability across our estimates indicate that a thorough analysis across all the river networks in the Sierra Nevada is necessary to robustly characterize the uplift history using these methods.

Signatures of tilt are robust to the extent that they are not obscured by other later-stage perturbations of greater magnitude. Heterogeneous lithology and deviations in the stream power exponent away from  $n = 1$  cause predictable deviations in the transient response to tilting, but generally do not completely obscure tilt signatures. In contrast, disequilibrium initial conditions and coincident perturbations may result in myriad permutations to predicted profile forms that may obscure signatures of tilt. To test the uniqueness of tilt signatures presented, we simulated a range of perturbations that generate transient river profiles that share characteristics with profiles generated by tilting, including a pulse of uniform uplift, step changes in fluvial relief, and mainstem beheading. Thus, although this paper focuses on tilting, it provides a detailed summary of the suite of signatures that characterize the transient fluvial response to each of these perturbations in longitudinal profiles,  $\chi$  plots, and patterns in mainstem incision below paleotopographic markers that could help to interpret more diverse landscape histories recorded in river network forms.

*Video supplement.* Videos showing response of model river network composed of linked 1-D river longitudinal profile evolution models to all perturbations discussed within are available as an online resource (see Beeson, 2019)

*Author contributions.* H.W.B and S.W.M designed the experiments and H.W.B developed the model code and performed the simulations. H.W.B conducted analysis on Sierra rivers. Both authors contributed to the writing of the manuscript

*Competing interests.* The authors declare that they have no conflict of interest.

*Acknowledgements.* We thank Taylor Perron for providing a 2D landscape evolution model that we modified for use in this paper.



## References

- Armstrong, P. A., Ehlers, T. A., Chapman, D. S., Farley, K. A., and Kamp, P. J. J.: Exhumation of the central Wasatch Mountains, Utah: 1. Patterns and timing of exhumation deduced from low-temperature thermochronology data, *Journal of Geophysical Research: Solid Earth*, 108, <https://doi.org/10.1029/2001JB001708>, 2003.
- 5 Attal, M., Cowie, P. A., Whittaker, A. C., Hobbey, D., Tucker, G. E., and Roberts, G. P.: Testing fluvial erosion models using the transient response of bedrock rivers to tectonic forcing in the Apennines, Italy, p. 17.
- Baldwin, J. A., Whipple, K. X., and Tucker, G. E.: Implications of the shear stress river incision model for the timescale of postorogenic decay of topography: Timescale of postorogenic decay, *Journal of Geophysical Research: Solid Earth*, 108, <https://doi.org/10.1029/2001JB000550>, 2003.
- 10 Bateman, P. and Wahrhaftig, C.: Geology of the Sierra Nevada, in: *Geology of Northern California*, vol. 190, pp. 107–172, California Division of Mines and Geology Bulletin, 1966.
- Beeson, H. W.: Geomorphic signatures of tilt: Animations of transient bedrock river response to perturbations, <https://doi.org/https://doi.org/10.6084/m9.figshare.8111498.v1>.
- Beeson, H. W., McCoy, S. W., and Keen-Zebert, A.: Geometric disequilibrium of river basins produces long-lived transient landscapes, *Earth and Planetary Science Letters*, 475, 34–43, <https://doi.org/10.1016/j.epsl.2017.07.010>, 2017.
- 15 Bonnet, S. and Crave, A.: Landscape response to climate change: Insights from experimental modeling and implications for tectonic versus climatic uplift of topography, *Geology*, 31, 123–126, 2003.
- Burbank, D. W., Leland, J., Fielding, E., Anderson, R. S., Brozovic, N., Reid, M. R., and Duncan, C.: Bedrock incision, rock uplift and threshold hillslopes in the northwestern Himalayas, *Nature*, 379, 505–510, <https://doi.org/10.1038/379505a0>, 1996.
- 20 Busby, C. J., Hagan, J. C., Putirka, K., Pluhar, C. J., Gans, P. B., Wagner, D. L., Rood, D., DeOreo, S. B., and Skilling, I.: The ancestral Cascades arc: Cenozoic evolution of the central Sierra Nevada (California) and the birth of the new plate boundary, in: *Special Paper 438: Ophiolites, Arcs, and Batholiths: A Tribute to Cliff Hopson*, vol. 438, pp. 331–378, Geological Society of America, [https://doi.org/10.1130/2008.2438\(12\)](https://doi.org/10.1130/2008.2438(12)), 2008.
- Byrd, J. O. D., Smith, R. B., and Geissman, J. W.: The Teton fault, Wyoming: Topographic signature, neotectonics, and mechanisms of deformation, *Journal of Geophysical Research: Solid Earth*, 99, 20 095–20 122, <https://doi.org/10.1029/94JB00281>, 1994.
- 25 Cassel, E. J., Graham, S. A., and Chamberlain, C. P.: Cenozoic tectonic and topographic evolution of the northern Sierra Nevada, California, through stable isotope paleoaltimetry in volcanic glass, *Geology*, 37, 547–550, <https://doi.org/10.1130/G25572A.1>, 2009.
- Cassel, E. J., Graham, S. A., Chamberlain, C. P., and Henry, C. D.: Early Cenozoic topography, morphology, and tectonics of the northern Sierra Nevada and western Basin and Range, *Geosphere*, 8, 229–249, 2012.
- 30 Cassel, E. J., Breecker, D. O., Henry, C. D., Larson, T. E., and Stockli, D. F.: Profile of a paleo-orogen: High topography across the present-day Basin and Range from 40 to 23 Ma, *Geology*, 42, 1007–1010, <https://doi.org/10.1130/G35924.1>, 2014.
- Christensen, M. N.: Late Cenozoic Crustal Movements in the Sierra Nevada of California, *Geological Society of America Bulletin*, 77, 163–182, [https://doi.org/10.1130/0016-7606\(1966\)77\[163:LCCMIT\]2.0.CO;2](https://doi.org/10.1130/0016-7606(1966)77[163:LCCMIT]2.0.CO;2), 1966.
- Clark, M. K., Maheo, G., Saleeby, J., and Farley, K. A.: The non-equilibrium landscape of the southern Sierra Nevada, California, *GSA Today*, 15, 4–10, 2005.
- 35 Curtis, G. H.: *Mode of origin of pyroclastic debris in the Mehrten formation of the Sierra Nevada.*, University of California Press., Berkeley., 1953.



- Delcaillau, B., Carozza, J.-M., and Laville, E.: Recent fold growth and drainage development: The Janauri and Chandigarh anticlines in the Siwalik foothills, northwest India, *Geomorphology*, 76, 241–256, <https://doi.org/10.1016/j.geomorph.2005.11.005>, 2006.
- DiBiase, R. A., Whipple, K. X., Heimsath, A. M., and Ouimet, W. B.: Landscape form and millennial erosion rates in the San Gabriel Mountains, CA, *Earth and Planetary Science Letters*, 289, 134–144, <https://doi.org/10.1016/j.epsl.2009.10.036>, 2010.
- 5 Ducea, M. N. and Saleeby, J. B.: Buoyancy sources for a large, unrooted mountain range, the Sierra Nevada, California: Evidence from xenolith thermobarometry, *Journal of Geophysical Research: Solid Earth*, 101, 8229–8244, <https://doi.org/10.1029/95JB03452>, 1996.
- Durrell, C.: Tertiary and Quaternary geology of the northern Sierra Nevada, in: Bailey, E.H., ed., *Geology of northern California*, vol. 190, pp. 185–197, California Division of Mines and Geology, 1966.
- Duvall, A., Kirby, E., and Burbank, D.: Tectonic and lithologic controls on bedrock channel profiles and processes in coastal California, *Journal of Geophysical Research: Earth Surface*, 109, F03 002, <https://doi.org/10.1029/2003JF000086>, 2004.
- 10 Fariás, M., Charrier, R., Comte, D., Martinod, J., and Hérail, G.: Late Cenozoic deformation and uplift of the western flank of the Altiplano: Evidence from the depositional, tectonic, and geomorphologic evolution and shallow seismic activity (northern Chile at 19°30'S), *Tectonics*, 24, n/a–n/a, <https://doi.org/10.1029/2004TC001667>, 2005.
- Ferrier, K. L., Huppert, K. L., and Perron, J. T.: Climatic control of bedrock river incision, *Nature*, 496, 206–209, <https://doi.org/10.1038/nature11982>, 2013.
- 15 Finnegan, N. J., Roe, G., Montgomery, D. R., and Hallet, B.: Controls on the channel width of rivers: Implications for modeling fluvial incision of bedrock, *Geology*, 33, 229, <https://doi.org/10.1130/G21171.1>, 2005.
- Flint, J. J.: Stream gradient as a function of order, magnitude, and discharge, *Water Resources Research*, 10, 969–973, <https://doi.org/10.1029/WR010i005p00969>, 1974.
- 20 Forte, A. M., Yanites, B. J., and Whipple, K. X.: Complexities of landscape evolution during incision through layered stratigraphy with contrasts in rock strength, *Earth Surface Processes and Landforms*, 41, 1736–1757, <https://doi.org/10.1002/esp.3947>, 2016.
- Gallen, S. F.: Lithologic controls on landscape dynamics and aquatic species evolution in post-orogenic mountains, *Earth and Planetary Science Letters*, 493, 150–160, <https://doi.org/10.1016/j.epsl.2018.04.029>, 2018.
- Goren, L.: A theoretical model for fluvial channel response time during time-dependent climatic and tectonic forcing and its inverse applications, *Geophysical Research Letters*, 43, 10,753–10,763, <https://doi.org/10.1002/2016GL070451>, 2016.
- 25 Gorynski, K. E., Stockli, D. F., and Douglas Walker, J.: Thermochronometrically constrained anatomy and evolution of a Miocene extensional accommodation zone and tilt domain boundary: The southern Wassuk Range, Nevada, *Tectonics*, 32, 516–539, <https://doi.org/10.1002/tect.20044>, 2013.
- Grimaud, J.-L., Paola, C., and Voller, V.: Experimental migration of knickpoints: influence of style of base-level fall and bed lithology, *Earth Surface Dynamics*, 4, 11–23, <https://doi.org/10.5194/esurf-4-11-2016>, 2016.
- 30 Hack, J.: *Studies of longitudinal stream profiles in Virginia and Maryland*, USGS Numbered Series 294-B, 1957.
- Haviv, I., Enzel, Y., Whipple, K. X., Zilberman, E., Matmon, A., Stone, J., and Fifield, K. L.: Evolution of vertical knickpoints (waterfalls) with resistant caprock: Insights from numerical modeling, *Journal of Geophysical Research: Earth Surface*, 115, <https://doi.org/10.1029/2008JF001187>, 2010.
- 35 Howard, A. D.: A detachment-limited model of drainage basin evolution, *Water Resources Research*, 30, 2261–2285, <https://doi.org/10.1029/94WR00757>, 1994.
- Howard, A. D. and Kerby, G.: Channel changes in badlands, *Geological Society of America Bulletin*, 94, 739–752, [https://doi.org/10.1130/0016-7606\(1983\)94<739:CCIB>2.0.CO;2](https://doi.org/10.1130/0016-7606(1983)94<739:CCIB>2.0.CO;2), 1983.



- Huber, N.: Amount and timing of late Cenozoic uplift and tilt of the central Sierra Nevada, California; evidence from the upper San Joaquin River basin, United States Geological Survey Professional Paper 1197, 1981.
- Jackson, J., van Dissen, R., and Berryman, K.: Tilting of active folds and faults in the Manawatu region, New Zealand: Evidence from surface drainage patterns, *New Zealand Journal of Geology and Geophysics*, 41, 377–385, <https://doi.org/10.1080/00288306.1998.9514817>, 1998.
- 5 Jones, C. H., Farmer, G. L., and Unruh, J.: Tectonics of Pliocene removal of lithosphere of the Sierra Nevada, California, *Geological Society of America Bulletin*, 116, 1408–1422, <https://doi.org/10.1130/B25397.1>, 2004.
- Jordan, T. E., Nester, P. L., Blanco, N., Hoke, G. D., Dávila, F., and Tomlinson, A. J.: Uplift of the Altiplano-Puna plateau: A view from the west, *Tectonics*, 29, n/a–n/a, <https://doi.org/10.1029/2010TC002661>, 2010.
- Kirby, E. and Whipple, K.: Quantifying differential rock-uplift rates via stream profile analysis, *Geology*, 29, 415,  
10 [https://doi.org/10.1130/0091-7613\(2001\)029<0415:QDRURV>2.0.CO;2](https://doi.org/10.1130/0091-7613(2001)029<0415:QDRURV>2.0.CO;2), 2001.
- Kirby, E. and Whipple, K. X.: Expression of active tectonics in erosional landscapes, *Journal of Structural Geology*, 44, 54–75, <https://doi.org/10.1016/j.jsg.2012.07.009>, 2012.
- Lague, D.: The stream power river incision model: evidence, theory and beyond: STREAM POWER INCISION MODEL, *Earth Surface Processes and Landforms*, 39, 38–61, <https://doi.org/10.1002/esp.3462>, 2014.
- 15 Lamb, S. and Hoke, L.: Origin of the high plateau in the central Andes, Bolivia, South America, *Tectonics*, 16, 623–649, <https://doi.org/10.1029/97TC00495>, 1997.
- Lavé, J. and Avouac, J. P.: Active folding of fluvial terraces across the Siwaliks Hills, Himalayas of central Nepal, *Journal of Geophysical Research: Solid Earth*, 105, 5735–5770, <https://doi.org/10.1029/1999JB900292>, 2000.
- Lease, R. O. and Ehlers, T. A.: Incision into the Eastern Andean Plateau During Pliocene Cooling, *Science*, 341, 774–776,  
20 <https://doi.org/10.1126/science.1239132>, 2013.
- Lindgren, W.: Tertiary gravels of the Sierra Nevada of California, United States Geological Survey Professional Paper 73, 1911.
- Liu, L. and Gurnis, M.: Dynamic subsidence and uplift of the Colorado Plateau, *Geology*, 38, 663–666, <https://doi.org/10.1130/G30624.1>, 2010.
- Ludington, S., Moring, B. C., Miller, R. J., and Flynn, K. S.: Preliminary Integrated Geologic Map Databases of the United States: The  
25 Western States: California, Nevada, Arizona, Washington, Idaho, Utah (OFR 2005-1305), 2005.
- Mackin, J. H.: Concept of the Graded River, *Geological Society of America Bulletin*, 59, 463–512, [https://doi.org/10.1130/0016-7606\(1948\)59\[463:COTGR\]2.0.CO;2](https://doi.org/10.1130/0016-7606(1948)59[463:COTGR]2.0.CO;2), 1948.
- McMillan, M. E., Angevine, C. L., and Heller, P. L.: Postdepositional tilt of the Miocene-Pliocene Ogallala Group on the western Great Plains: Evidence of late Cenozoic uplift of the Rocky Mountains, *Geology*, 30, 63, [https://doi.org/10.1130/0091-7613\(2002\)030<0063:PTOTMP>2.0.CO;2](https://doi.org/10.1130/0091-7613(2002)030<0063:PTOTMP>2.0.CO;2), 2002.  
30
- McPhillips, D. and Brandon, M. T.: Topographic evolution of the Sierra Nevada measured directly by inversion of low-temperature thermochronology, *American Journal of Science*, 312, 90–116, 2012.
- Mitchell, N. and Yanites, B.: Spatially variable increase in rock uplift in the northern U.S. Cordillera recorded in the distribution of river knickpoints and incision depths, *Journal of Geophysical Research: Earth Surface*, 0, <https://doi.org/10.1029/2018JF004880>.
- 35 Molnar, P.: Deuterium and oxygen isotopes, paleoelevations of the Sierra Nevada, and Cenozoic climate, *Geological Society of America Bulletin*, 122, 1106–1115, <https://doi.org/10.1130/B30001.1>, 2010.
- Moucha, R., Forte, A. M., Rowley, D. B., Mitrovica, J. X., Simmons, N. A., and Grand, S. P.: Mantle convection and the recent evolution of the Colorado Plateau and the Rio Grande Rift valley, *Geology*, 36, 439–442, <https://doi.org/10.1130/G24577A.1>, 2008.



- Moucha, R., Forte, A. M., Rowley, D. B., Mitrovica, J. X., Simmons, N. A., and Grand, S. P.: Deep mantle forces and the uplift of the Colorado Plateau, *Geophysical Research Letters*, 36, <https://doi.org/10.1029/2009GL039778>, 2009.
- Ouimet, W. B., Whipple, K. X., and Granger, D. E.: Beyond threshold hillslopes: Channel adjustment to base-level fall in tectonically active mountain ranges, *Geology*, 37, 579–582, 2009.
- 5 Pelletier, J. D.: Numerical modeling of the Cenozoic geomorphic evolution of the southern Sierra Nevada, California, *Earth and Planetary Science Letters*, 259, 85–96, <https://doi.org/10.1016/j.epsl.2007.04.030>, 2007.
- Perron, J. T. and Royden, L.: An integral approach to bedrock river profile analysis, *Earth Surface Processes and Landforms*, 38, 570–576, <https://doi.org/10.1002/esp.3302>, 2013.
- Perron, J. T., Dietrich, W. E., and Kirchner, J. W.: Controls on the spacing of first-order valleys, *Journal of Geophysical Research: Earth Surface*, 113, F04 016, <https://doi.org/10.1029/2007JF000977>, 2008.
- 10 Riihimaki, C. A., Anderson, R. S., and Safran, E. B.: Impact of rock uplift on rates of late Cenozoic Rocky Mountain river incision, *Journal of Geophysical Research*, 112, <https://doi.org/10.1029/2006JF000557>, 2007.
- Rosenbloom, N. A. and Anderson, R. S.: Hillslope and channel evolution in a marine terraced landscape, Santa Cruz, California, *Journal of Geophysical Research: Solid Earth*, 99, 14 013–14 029, <https://doi.org/10.1029/94JB00048>, 1994.
- 15 Royden, L. and Perron, J. T.: Solutions of the stream power equation and application to the evolution of river longitudinal profiles, *Journal of Geophysical Research: Earth Surface*, 118, 497–518, <https://doi.org/10.1002/jgrf.20031>, 2013.
- Sahagian, D., Proussevitch, A., and Carlson, W.: Timing of Colorado Plateau uplift: Initial constraints from vesicular basalt-derived paleo-elevations, *Geology*, 30, 807, [https://doi.org/10.1130/0091-7613\(2002\)030<0807:TOCPUI>2.0.CO;2](https://doi.org/10.1130/0091-7613(2002)030<0807:TOCPUI>2.0.CO;2), 2002.
- Saylor, J. E. and Horton, B. K.: Nonuniform surface uplift of the Andean plateau revealed by deuterium isotopes in Miocene volcanic glass from southern Peru, *Earth and Planetary Science Letters*, 387, 120–131, <https://doi.org/10.1016/j.epsl.2013.11.015>, 2014.
- 20 Schwanghart, W. and Scherler, D.: Short Communication: TopoToolbox 2 – MATLAB-based software for topographic analysis and modeling in Earth surface sciences, *Earth Surface Dynamics*, 2, 1–7, <https://doi.org/https://doi.org/10.5194/esurf-2-1-2014>, 2014.
- Siedl, M. and Dietrich, W. E.: The problem of channel erosion into bedrock, *Catena Supplement*, 23, 101–124, 1992.
- Singh, V. and Tandon, S. K.: Evidence and consequences of tilting of two alluvial fans in the Pinjaur dun, Northwestern Himalayan Foothills, *Quaternary International*, 159, 21–31, <https://doi.org/10.1016/j.quaint.2006.08.017>, 2007.
- 25 Sklar, L. and Dietrich, W. E.: River Longitudinal Profiles and Bedrock Incision Models: Stream Power and the Influence of Sediment Supply, in: *Rivers Over Rock: Fluvial Processes in Bedrock Channels*, edited by Tinkler, K. J. and Wohl, E. E., pp. 237–260, American Geophysical Union, 1998.
- Sklar, L. S. and Dietrich, W. E.: A mechanistic model for river incision into bedrock by saltating bed load, *Water Resources Research*, 40, W06 301, <https://doi.org/10.1029/2003WR002496>, 2004.
- 30 Slemmons, D.: Cenozoic volcanism of the central Sierra Nevada, California, in: Bailey, E.H., ed., *Geology of northern California*, vol. 90, pp. 199–208, California Division of Mines and Geology, 1966.
- Snyder, N. P.: Landscape response to tectonic forcing: Digital elevation model analysis of stream profiles in the Mendocino triple junction region, northern California, *Geological Society of America Bulletin*, p. 14, 2000.
- 35 Snyder, N. P., Whipple, K. X., Tucker, G. E., and Merritts, D. J.: Interactions between onshore bedrock-channel incision and nearshore wave-base erosion forced by eustasy and tectonics, *Basin Research*, 14, 105–127, <https://doi.org/10.1046/j.1365-2117.2002.00169.x>, 2002.
- Stewart, J. H.: Regional tilt patterns of late Cenozoic basin-range fault blocks, western United States, *GSA Bulletin*, 91, 460–464, [https://doi.org/10.1130/0016-7606\(1980\)91<460:RTPOLC>2.0.CO;2](https://doi.org/10.1130/0016-7606(1980)91<460:RTPOLC>2.0.CO;2), 1980.



- Stock, G. M., Anderson, R. S., and Finkel, R. C.: Pace of landscape evolution in the Sierra Nevada, California, revealed by cosmogenic dating of cave sediments, *Geology*, 32, 193–196, <https://doi.org/10.1130/G20197.1>, 2004.
- Stock, G. M., Anderson, R. S., and Finkel, R. C.: Rates of erosion and topographic evolution of the Sierra Nevada, California, inferred from cosmogenic  $^{26}\text{Al}$  and  $^{10}\text{Be}$  concentrations, *Earth Surface Processes and Landforms*, 30, 985–1006, <https://doi.org/10.1002/esp.1258>,  
5 2005.
- Stock, J. and Dietrich, W. E.: Valley incision by debris flows: Evidence of a topographic signature, *Water Resources Research*, 39, n/a–n/a, <https://doi.org/10.1029/2001WR001057>, 2003.
- Stock, J. D. and Montgomery, D. R.: Geologic constraints on bedrock river incision using the stream power law, *Journal of Geophysical Research: Solid Earth*, 104, 4983–4993, <https://doi.org/10.1029/98JB02139>, 1999.
- 10 Stockli, D. F., Dumitru, T. A., McWilliams, M. O., and Farley, K. A.: Cenozoic tectonic evolution of the White Mountains, California and Nevada, *Geological Society of America Bulletin*, 115, 788–816, [https://doi.org/10.1130/0016-7606\(2003\)115<0788:CTEOTW>2.0.CO;2](https://doi.org/10.1130/0016-7606(2003)115<0788:CTEOTW>2.0.CO;2), 2003.
- Tucker, G. E. and Whipple, K. X.: Topographic outcomes predicted by stream erosion models: Sensitivity analysis and intermodel comparison, *Journal of Geophysical Research*, 107, <https://doi.org/10.1029/2001JB000162>, 2002.
- 15 Turowski, J. M., Lague, D., and Hovius, N.: Response of bedrock channel width to tectonic forcing: Insights from a numerical model, theoretical considerations, and comparison with field data, *Journal of Geophysical Research: Earth Surface*, 114, <https://doi.org/10.1029/2008JF001133>, 2009.
- Unruh, J. R.: The uplift of the Sierra Nevada and implications for late Cenozoic epeirogeny in the western Cordillera, *Geological Society of America Bulletin*, 103, 1395–1404, [https://doi.org/10.1130/0016-7606\(1991\)103<1395:TUOTSN>2.3.CO;2](https://doi.org/10.1130/0016-7606(1991)103<1395:TUOTSN>2.3.CO;2), 1991.
- 20 Wakabayashi, J.: Paleochannels, stream incision, erosion, topographic evolution, and alternative explanations of paleoaltimetry, *Sierra Nevada, California*, *Geosphere*, 9, 191–215, 2013.
- Wakabayashi, J. and Sawyer, T. L.: Stream Incision, Tectonics, Uplift, and Evolution of Topography of the Sierra Nevada, California, *The Journal of Geology*, 109, 539–562, <https://doi.org/10.1086/321962>, 2001.
- Whipple, K., DiBiase, R., and Crosby, B.: 9.28 Bedrock Rivers, in: *Treatise on Geomorphology*, pp. 550–573, Elsevier,  
25 <https://doi.org/10.1016/B978-0-12-374739-6.00254-2>, 2013.
- Whipple, K. X.: Bedrock Rivers and the Geomorphology of Active Orogens, *Annual Review of Earth and Planetary Sciences*, 32, 151–185, <https://doi.org/10.1146/annurev.earth.32.101802.120356>, 2004.
- Whipple, K. X. and Tucker, G. E.: Dynamics of the stream-power river incision model: Implications for height limits of mountain ranges, landscape response timescales, and research needs, *Journal of Geophysical Research: Solid Earth*, 104, 17 661–17 674,  
30 <https://doi.org/10.1029/1999JB900120>, 1999.
- Whipple, K. X. and Tucker, G. E.: Implications of sediment-flux-dependent river incision models for landscape evolution, *Journal of Geophysical Research: Solid Earth*, 107, ETG 3–1, <https://doi.org/10.1029/2000JB000044>, 2002.
- Whipple, K. X., Hancock, G. S., and Anderson, R. S.: River incision into bedrock: Mechanics and relative efficacy of plucking, abrasion, and cavitation, *GSA Bulletin*, 112, 490–503, [https://doi.org/10.1130/0016-7606\(2000\)112<490:RIIBMA>2.0.CO;2](https://doi.org/10.1130/0016-7606(2000)112<490:RIIBMA>2.0.CO;2), 2000.
- 35 Whipple, K. X., Forte, A. M., DiBiase, R. A., Gasparini, N. M., and Ouimet, W. B.: Timescales of landscape response to divide migration and drainage capture: Implications for the role of divide mobility in landscape evolution: *Landscape Response to Divide Mobility*, *Journal of Geophysical Research: Earth Surface*, 122, 248–273, <https://doi.org/10.1002/2016JF003973>, 2017.



- Whittaker, A. C., Cowie, P. A., Attal, M., Tucker, G. E., and Roberts, G. P.: Bedrock channel adjustment to tectonic forcing: Implications for predicting river incision rates, *Geology*, 35, 103, <https://doi.org/10.1130/G23106A.1>, 2007.
- Whittaker, A. C., Attal, M., Cowie, P. A., Tucker, G. E., and Roberts, G.: Decoding temporal and spatial patterns of fault uplift using transient river long profiles, *Geomorphology*, 100, 506–526, <https://doi.org/10.1016/j.geomorph.2008.01.018>, 2008.
- 5 Willett, S. D., McCoy, S. W., Perron, J. T., Goren, L., and Chen, C.-Y.: Dynamic Reorganization of River Basins, *Science*, 343, 1248–1252, <https://doi.org/10.1126/science.1248765>, 2014.
- Willett, S. D., McCoy, S. W., and Beeson, H. W.: Transience of the North American High Plains landscape and its impact on surface water, *Nature*, 561, 528–532, <https://doi.org/10.1038/s41586-018-0532-1>, 2018.
- Wobus, C. W., Tucker, G. E., and Anderson, R. S.: Self-formed bedrock channels, *Geophysical Research Letters*, 33, <https://doi.org/10.1029/2006GL027182>, 2006.
- 10 Wörner, G., Uhlig, D., Kohler, I., and Seyfried, H.: Evolution of the West Andean Escarpment at 18°S (N. Chile) during the last 25 Ma: uplift, erosion and collapse through time, *Tectonophysics*, 345, 183–198, [https://doi.org/10.1016/S0040-1951\(01\)00212-8](https://doi.org/10.1016/S0040-1951(01)00212-8), 2002.
- Yang, R., Willett, S. D., and Goren, L.: In situ low-relief landscape formation as a result of river network disruption, *Nature*, 520, 526–529, <https://doi.org/10.1038/nature14354>, 2015.
- 15 Yanites, B. J. and Tucker, G. E.: Controls and limits on bedrock channel geometry, *Journal of Geophysical Research: Earth Surface*, 115, <https://doi.org/10.1029/2009JF001601>, 2010.
- Yanites, B. J., Tucker, G. E., Mueller, K. J., Chen, Y.-G., Wilcox, T., Huang, S.-Y., and Shi, K.-W.: Incision and channel morphology across active structures along the Peikang River, central Taiwan: Implications for the importance of channel width, *Geological Society of America Bulletin*, 122, 1192–1208, <https://doi.org/10.1130/B30035.1>, 2010.
- 20 Yeend, W. E.: Gold-bearing gravel of the ancestral Yuba River, Sierra Nevada, California, United States Geological Survey Professional Paper 772, 1974.